Ore Geology Reviews 144 (2022) 104848

Contents lists available at ScienceDirect

Ore Geology Reviews

journal homepage: www.elsevier.com/locate/oregeorev

Geochemical characteristics and paleoclimate implication of Middle Jurassic coal in the Ordos Basin, China

Luojing Wang [a], Dawei Lv [a,*], James C. Hower [b], Zhihui Zhang [a], Munira Raji [c], Jigen Tang [d], Yamin Liu [d], Jie Gao [a]

[a] Shandong Provincial Key Laboratory of Depositional Mineralization and Sedimentary Minerals, College of Earth Sciences and Engineering, Shandong University of Science and Technology, Qingdao 266590, PR China
[b] University of Kentucky, Center for Applied Energy Research, 2540 Research Park Drive, Lexington, KY 40511, United States of America
[c] University of Portsmouth, School of The Environment, Geography and Geosciences, St. Michael's Building, White Swan Road, Portsmouth PO1 2DT, United Kingdom
[d] The Sixth Gas Production Plant, PetroChina Changqing Oilfield Company, Xi'an 710018, PR China

ARTICLE INFO

Keywords:
Coal
Yan'an Formation
Trace elements
Jurassic
Paleoclimate

ABSTRACT

Coals are highly enriched in critical elements (rare earth elements, etc.), containing much information of paleoenvironmental and paleoclimatic during deposition. The Jurassic period is a significant coal-forming period in the world. The Yan'an Formation in the Ordos Basin in north China is among the largest Middle Jurassic coal fields of the world. The purpose of this study is to investigate the geochemical characteristics of Middle Jurassic Aalenian coals of Ordos Basin and their paleoclimate significance. Sixty-two coal samples were collected from two coal mines in the Dongsheng area in the northeast Ordos Basin. The major and trace elements in the coal samples were analyzed using X-ray fluorescence (XRF) and inductively coupled plasma-mass spectrometry (ICP-MS). The main oxides in the Yan'an coals are SiO_2 and CaO. In comparison with average values for China, the coals from the Ordos Basin have a slight enrichment of CaO and MgO. Strontium and Mo values are also slightly enriched. Yttrium and rare earth elements are depleted in the coals, with a range of 8–269 μg/g (average = 48.5 μg/g; on an ash basis). The coals in the Yan'an Formation have a negative Eu anomaly, suggesting that the peat bog had a stable terrigenous material supply during the coal-forming period. The continental saline water system and oxygen-suboxygenic environment were inferred from the Sr/Ba, U/Th, Ni/Co, Sr/Cu. The Sr/Cu and Sr/Ba data of Yan'an Formation coal seams in the Ordos Basin also indicate climate change from a relatively arid condition to a more humid climate, which is consistent with change of marine environment during the Aalenian. Global cooling during the Aalenian may have triggered strengthened moisture transport by westerlies in mid-latitude inland Asia, and therefore a humid climate in the Ordos Basin.

1. Introduction

Coal is a significant mineral and economic resource in many countries globally (Scott et al., 2007; Dai and Finkelman, 2018; Dai et al., 2020). It is the major source and material for power generation, energy-intensive industries (steel, cement, etc.), and residential and commercial heating (Chang et al., 2016). In addition, coals are highly enriched in critical elements, including Ge, Ga, U, V, Se, rare earth elements and Y (REY or REE if Y is not included), Sc, Y, Au, and Ag, as well as base metals, such as Al and Mg (Dai and Finkelman, 2018). Coal and coal byproducts are substantially enhanced with trace metals and have been proposed as a promising source recovery option of REEs in recent years (Liu et al., 2019; Eterigho-Ikelegbe et al., 2021). Coal utilization is mostly based on its chemical properties (Dai et al., 2020). Trace elements such as Hg, As, and Se present in coal are known to be of concern for public health (Bhangare et al., 2011). In addition, coal is a major source of greenhouse gases (GHGs) and air pollutants (Chang et al., 2016). Therefore, it is vital to identify the enrichment and distribution of coal elements.

Coal records significant paleoenvironment and paleoclimate information during geological and historical periods (Ferm et al., 1979; Hautevelle et al., 2006; Dai et al., 2020; Mathews et al., 2020). Many of the elements in coals were formed during the sedimentary stages, reflecting the paleoenvironments and paleoclimate (Lv et al., 2019; Dai

* Corresponding author.
E-mail address: lvdawei95@126.com (D. Lv).

https://doi.org/10.1016/j.oregeorev.2022.104848
Received 29 December 2021; Received in revised form 25 February 2022; Accepted 20 March 2022
Available online 25 March 2022

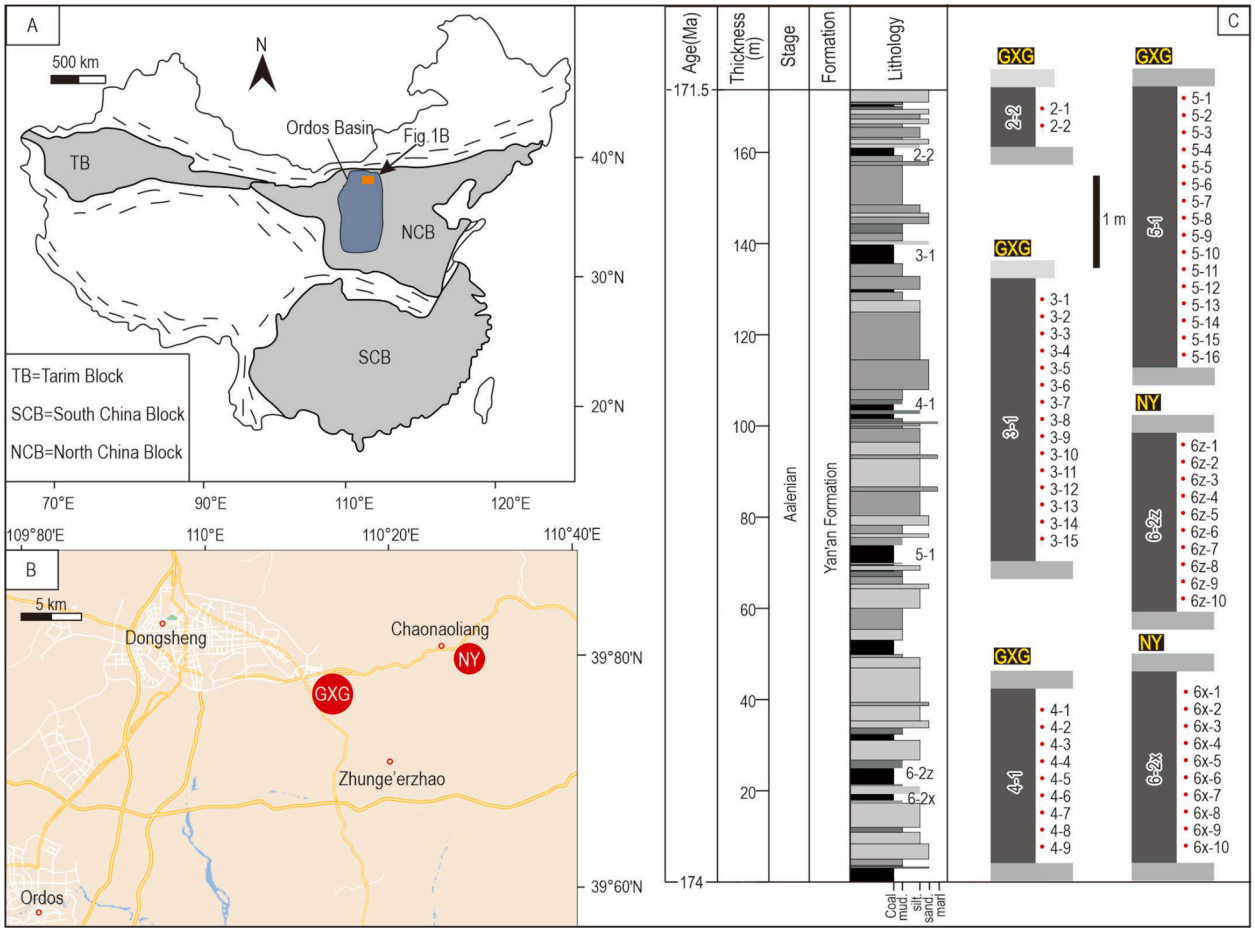

Fig. 1. Geological settings and strata of the study area. (A) The location of the Ordos Basin. (B) Geologic map of the study area showing the position of the studied mining area. GXG is Gaoxigou; NY is Nayuan. (C) Stratigraphic column of the Yan'an Formation (Zhang et al., 2021).

et al., 2020; Gayer et al., 1999). The physical and chemical properties of coal are also mostly determined by the depositional environment after the peat was formed (Dai et al., 2020). Therefore, it is significant to study the coal geochemical composition and enrichment of major and trace elements to understand the mechanisms of coal formation and paleoclimate change.

The Ordos Basin is one of the most prominent Chinese inland coal-accumulating basins in the Jurassic period (Wang et al., 1996). The Middle-Lower Jurassic Yan'an Formation has many coal seams, which can be tracked through the whole basin (Wang et al., 1996). Several studies have been carried out on sedimentary facies and coal accumulation rules (Zhang et al., 1995; Wang and Zhang, 1999). There are also some studies which focused on petrology and element geochemistry of coal in the Ordos Basin (Liu et al., 2007; Qin et al., 2015; Wang et al., 2011), but little information is available on the variation of sedimentary environments during coal formation and accumulation.

The primary aim of this study is to probe into the geochemical characteristics and paleoenvironment for the coal seams based on broad research on element geochemistry of coals from the Dongsheng area in the northwest Ordos Basin. A recent study by Zhang et al. (2021) suggests that the depositional period of the Yan'an Formation in the Ordos Basin may have been in the cooling period after the Toarcian Oceanic Anoxic Event. Some researchers also pointed out that the short-term rapid cooling event in the early Aalenian stage may have a particular impact on the enrichment of terrestrial organic carbon (Dromart et al., 2003; Rogov and Zakharov, 2010; Dera et al., 2011). Thus, it is significant to study the influence of the cooling events on the coal seams development of the Yan'an Formation in the Ordos Basin to reveal the early and middle Jurassic land paleoclimate changes in Eastern Asia.

2. Geological setting

The Ordos Basin, with an area of 250,000 km^2, is the second-largest sedimentary basin in China. Located in central and western China and the western part of the North China Craton (Fig. 1A), it covers three provinces and two autonomous regions. It is surrounded by mountain belts and fault (rift) basins: Qinling Mountain/Weifen Basin to the south, Liupan and Helan Mountains/Yinchuan Basin to the west, and Daqing and Lvliang Mountains/Yuncheng Basin to the east (Yin et al., 1990).

The Ordos Basin is famous for its vast energy resources (coal, oil, and gas), and the widely distributed Jurassic coal accounts for a large part of the total coal in the Ordos Basin (Ao et al., 2012; . The sedimentary cap layer in the Ordos Basin began to develop from the Cambrian period. The crystalline substrate is the most stable structural unit in Craton, North China. The intra-cratonic Ordos Basin is filled with middle upper Proterozoic to Cenozoic sediments underlain by an Archean to lower Proterozoic basement (Akhtar et al., 2017). The formation and evolution of the Ordos Basin is also closely related to the tectonic development of craton in North China, influenced by the Late Triassic Indochina orogeny, Jurassic Yanshan orogeny, and the late Cenozoic Himalayan orogeny (Johnson et al., 1989).

The study area is located in the coal mine in the Dongsheng District (Ordos City, Inner Mongolia). The Yan'an Formation, with an exposed area of ca. 2000 km^2, is well developed in the Dongsheng coalfield unconformably overlies the the Triassic (and older) strata in most outcrops (Zhang et al., 2021). Overall, the Dongsheng area is a stable

Table 1
Major element oxides of coal samples in Yan'an Formation (%; on whole coal/rock basis).

Coal seam	Sample	SiO_2	Al_2O_3	Fe_3O_2	MgO	CaO	Na_2O	K_2O	MnO	TiO_2	P_2O_5
2–2	2–1	6.59	2.77	0.79	0.43	2.66	0.07	0.06	0.02	0.27	0.01
	2–2	6.15	3.92	0.90	0.40	2.29	0.03	0.03	0.02	0.36	0.02
3–1	3–1	4.64	5.25	0.76	0.64	2.71	0.05	0.06	0.01	0.31	0.02
	3–2	1.18	0.46	0.88	0.50	2.36	0.05	0.03	0.01	0.03	0.01
	3–3	4.52	1.04	0.23	0.60	3.17	0.05	0.04	0.01	0.08	0.01
	3–4	1.22	0.53	0.68	0.55	2.60	0.07	0.02	0.01	0.04	0.01
	3–5	2.22	0.59	0.21	0.58	3.30	0.12	0.06	0.01	0.06	0.01
	3–6	1.48	0.58	0.58	0.42	2.04	0.06	0.03	0.01	0.05	0.01
	3–7	1.40	0.48	0.27	0.42	2.13	0.05	0.02	0.03	0.04	0.01
	3–8	2.82	1.16	1.77	0.53	2.06	0.11	0.06	0.02	0.05	0.01
	3–9	3.21	5.11	1.03	0.56	2.09	0.09	0.05	0.03	0.33	0.03
	3–10	5.16	14.01	1.68	0.58	1.98	0.09	0.14	0.04	0.66	0.07
	3–11	8.32	1.14	1.95	0.36	1.93	0.07	0.02	0.02	0.10	0.01
	3–12	3.86	0.85	0.30	0.36	1.72	0.06	0.02	0.02	0.05	0.01
	3–13	0.55	0.72	0.47	0.42	1.88	0.06	0.02	0.01	0.08	0.01
	3–14	1.14	1.16	0.93	0.43	2.20	0.04	0.02	0.01	0.03	0.01
	3–15	1.51	1.42	0.72	0.38	1.69	0.07	0.04	0.01	0.06	0.01
4–1	4–1	0.57	0.79	0.95	0.26	1.73	0.28	0.03	0.01	0.02	0.01
	4–2	17.81	7.37	2.32	0.70	1.94	0.26	0.84	0.02	0.31	0.04
	4–3	4.01	1.06	0.66	0.30	2.13	0.15	0.08	0.01	0.11	0.01
	4–4	5.18	2.39	1.66	0.31	2.06	0.18	0.09	0.02	0.18	0.02
	4–5	2.28	0.62	0.50	0.35	2.67	0.14	0.05	0.02	0.08	0.01
	4–6	10.18	4.19	0.81	0.39	1.64	0.19	0.45	0.01	0.24	0.03
	4–7	1.50	0.81	0.54	0.30	2.09	0.16	0.05	0.02	0.05	0.01
	4–8	1.73	0.73	0.45	0.33	2.31	0.14	0.04	0.01	0.05	0.01
	4–9	2.81	1.13	0.55	0.37	2.40	0.14	0.07	0.02	0.08	0.04
5–1	5–1	1.83	0.79	1.13	0.35	2.16	0.12	0.02	0.01	0.04	0.01
	5–2	9.29	3.49	0.32	0.38	2.06	0.11	0.17	0.01	0.17	0.01
	5–3	0.95	0.74	0.94	0.32	1.67	0.13	0.02	0.01	0.04	0.01
	5–4	0.97	0.55	0.55	0.38	2.20	0.09	0.03	0.02	0.03	0.04
	5–5	1.40	0.65	0.76	0.38	1.96	0.12	0.02	0.01	0.05	0.01
	5–6	2.10	0.65	0.86	0.40	2.22	0.12	0.05	0.02	0.05	0.01
	5–7	4.83	1.00	0.28	0.39	2.66	0.11	0.02	0.01	0.10	0.01
	5–8	1.47	0.72	0.63	0.38	1.76	0.12	0.03	0.01	0.05	0.01
	5–9	2.40	1.02	0.28	0.38	2.27	0.10	0.02	0.01	0.09	0.01
	5–10	1.34	1.66	0.39	0.38	1.83	0.13	0.02	0.02	0.08	0.01
	5–11	2.35	1.98	0.13	0.38	1.94	0.10	0.02	0.01	0.09	0.01
	5–12	0.97	1.03	0.17	0.36	1.92	0.09	0.01	0.02	0.06	0.01
	5–13	0.67	0.60	0.19	0.34	1.90	0.09	0.01	0.02	0.04	0.01
	5–14	1.26	0.33	0.75	0.30	1.87	0.09	0.01	0.02	0.04	0.01
	5–15	1.34	0.51	1.64	0.28	1.65	0.11	0.01	0.02	0.02	0.01
	5–16	3.84	1.04	0.70	0.30	1.53	0.11	0.03	0.01	0.06	0.01
6-2z	6z-1	4.52	1.43	0.21	0.54	2.76	0.06	0.01	0.01	0.07	0.01
	6z-2	4.44	2.16	0.20	0.54	2.70	0.07	0.01	0.01	0.20	0.01
	6z-3	2.15	0.57	1.65	0.50	2.76	0.08	0.02	0.01	0.04	0.09
	6z-4	0.94	0.46	3.31	0.41	2.37	0.06	0.01	0.01	0.02	0.20
	6z-5	1.86	1.16	0.56	0.51	2.55	0.06	0.02	0.01	0.04	0.06
	6z-6	2.19	0.84	0.42	0.54	2.82	0.07	0.02	0.01	0.04	0.03
	6z-7	1.45	0.57	0.34	0.48	2.48	0.06	0.01	0.01	0.03	0.04
	6z-8	1.98	0.55	1.42	0.44	2.25	0.06	0.01	0.01	0.04	0.02
	6z-9	1.08	0.40	0.42	0.46	2.36	0.07	0.01	0.01	0.02	0.01
	6z-10	1.65	1.08	0.93	0.53	2.98	0.07	0.01	0.01	0.03	0.01
6-2x	6x-1	4.32	1.93	0.38	0.50	2.66	0.06	0.01	0.01	0.10	0.01
	6x-2	2.85	1.26	0.20	0.53	2.94	0.06	0.01	0.01	0.05	0.01
	6x-3	2.11	1.24	0.31	0.57	3.22	0.07	0.02	0.01	0.04	0.01
	6x-4	1.64	1.12	0.21	0.53	2.67	0.06	0.02	0.01	0.04	0.05
	6x-5	1.51	1.04	0.75	0.48	7.48	0.05	0.02	0.15	0.06	0.16
	6x-6	4.61	3.63	0.36	0.58	3.64	0.08	0.02	0.02	0.04	0.02
	6x-7	2.72	1.75	0.49	0.55	3.02	0.09	0.02	0.01	0.06	0.31
	6x-8	2.38	1.69	0.38	0.57	3.65	0.07	0.02	0.01	0.06	0.27
	6x-9	2.86	2.17	1.40	0.52	5.97	0.12	0.04	0.01	0.05	2.27
	6x-10	21.68	14.70	1.87	0.48	3.09	0.05	0.07	0.01	0.29	0.04
	GM	11.06	1.93	0.77	0.44	2.48	0.09	0.05	0.02	0.10	0.07
	CWA	8.47	5.98	4.85	0.22	1.23	0.16	0.19	0.02	0.33	0.09

GM: Geometric average content CWA: Average values for China coals (Dai et al., 2012).

southeastern-dipping homocline.

There are many Jurassic outcrops in the Dongsheng and Zhungeer areas on the northeastern margin of the Ordos Basin (Li et al., 1995). However, the coal seams in the Yan'an Formation of the Middle Jurassic are the main target layers of this study. The lithology of the Yan'an Formation is composed of gray sandstone and coal seams (Fig. 1C), with a few interlayers of mudstone and silt. The Yan'an Formation is well developed in the Dongsheng area with a thickness of 133–279 m. Therefore, it is a suitable locality for analyzing the variations in coal seams' geochemical characteristics in response to the sedimentary environment's evolution.

Table 2
Trace elements of coal samples in Yan'an Formation (μg/g).

Coal seam	Sample	Li	Be	Sc	V	Cr	Co	Ni	Cu	Zn	Ga	Rb	Sr	Mo	Cd	In
2–1	2–1	5.40	0.42	4.01	34.40	17.10	4.15	21.80	48.70	18.70	3.18	1.80	117.00	0.94	0.07	0.03
	2–2	8.27	0.68	5.24	49.60	19.50	3.68	8.22	10.40	12.60	6.98	1.05	115.00	1.76	0.09	0.02
3–1	3–1	26.90	10.90	4.79	97.20	25.30	3.00	7.61	6.87	10.20	6.94	1.37	732.00	0.39	0.03	0.02
	3–2	1.19	0.86	0.32	61.30	7.34	6.89	5.68	3.06	5.25	2.38	0.72	508.00	4.16	0.06	0.01
	3–3	3.34	0.16	0.52	66.80	7.69	2.10	3.59	15.70	9.01	1.05	0.94	787.00	0.27	0.03	0.01
	3–4	1.43	0.11	0.40	42.50	5.18	7.22	23.80	25.10	11.50	1.00	0.48	543.00	0.74	0.05	0.01
	3–5	2.12	0.14	0.78	95.50	8.93	2.42	4.07	5.57	11.10	1.25	2.52	819.00	0.41	0.04	0.02
	3–6	1.18	0.08	0.36	62.80	4.94	5.15	10.60	4.76	8.09	1.31	1.08	460.00	1.67	0.02	0.01
	3–7	1.58	0.07	0.39	90.90	6.45	0.53	4.87	3.01	3.65	0.98	0.48	478.00	0.87	0.01	0.01
	3–8	2.92	0.14	0.80	79.90	6.34	2.14	4.33	4.72	8.63	1.34	1.34	410.00	2.85	0.05	0.01
	3–9	21.30	1.30	7.51	107.00	34.90	1.98	10.10	30.10	27.70	11.20	3.61	568.00	3.52	0.08	0.03
	3–10	12.90	0.43	1.94	91.20	20.50	1.13	5.40	5.63	10.20	5.47	1.14	488.00	1.19	0.03	0.02
	3–11	6.75	0.11	0.91	96.60	10.10	0.75	3.79	4.08	3.87	1.40	0.44	429.00	2.55	0.05	0.01
	3–12	4.86	0.13	0.60	48.10	5.58	0.50	3.87	2.01	3.08	1.11	0.60	397.00	1.06	0.01	0.01
	3–13	1.37	0.14	0.48	61.90	7.67	1.01	9.05	17.80	9.83	2.24	0.29	422.00	0.52	0.02	0.02
	3–14	1.93	2.43	0.74	48.70	4.59	4.69	7.47	3.33	2.68	2.07	0.41	443.00	0.33	0.02	0.01
	3–15	2.05	5.74	2.76	45.40	9.60	3.53	8.14	23.20	2.65	13.10	1.10	396.00	0.45	0.02	0.02
4–1	4–1	1.07	3.80	1.07	38.50	4.00	3.47	9.19	1.97	2.61	12.00	0.51	411.00	2.32	0.02	0.01
	4–2	9.80	4.77	7.18	89.70	25.60	6.47	22.40	31.30	26.50	8.16	30.70	503.00	1.15	0.19	0.04
	4–3	2.19	1.70	1.36	39.30	6.95	5.71	13.90	19.10	11.70	1.99	2.35	479.00	1.21	0.03	0.01
	4–4	5.19	0.25	1.66	28.00	8.01	7.05	13.20	13.40	10.50	2.29	1.63	445.00	2.01	0.06	0.02
	4–5	1.51	2.24	0.93	64.90	7.33	5.83	15.00	30.50	12.80	1.40	1.10	562.00	0.65	0.06	0.01
	4–6	6.23	1.51	12.00	151.00	74.50	4.43	9.89	27.00	10.40	18.60	20.60	449.00	1.38	0.06	0.05
	4–7	1.07	1.35	1.55	42.30	6.43	8.11	11.80	18.40	11.70	2.80	1.01	464.00	0.86	0.02	0.01
	4–8	0.93	1.24	0.99	17.90	6.13	7.30	8.62	18.50	9.49	1.87	1.26	535.00	0.79	0.02	0.01
	4–9	2.31	1.49	1.32	51.70	9.42	5.47	6.92	18.20	10.60	2.22	2.26	532.00	0.64	0.04	0.01
5–1	5–1	0.82	5.68	2.85	9.76	3.69	14.20	10.40	2.97	2.57	6.14	0.39	474.00	0.65	0.01	0.02
	5–2	3.10	1.24	2.67	29.70	20.20	7.46	6.52	13.70	6.53	3.63	5.82	521.00	0.39	0.04	0.02
	5–3	0.93	0.26	0.53	28.20	3.32	10.10	7.46	2.65	1.99	1.26	0.51	430.00	1.29	0.01	0.01
	5–4	1.33	0.11	0.39	14.70	3.08	3.37	7.00	17.50	13.70	0.94	0.67	521.00	0.42	0.04	0.01
	5–5	1.45	0.11	0.49	22.40	3.02	2.15	5.47	4.52	3.75	0.77	0.45	462.00	0.25	0.02	0.01
	5–6	1.25	0.07	0.44	19.20	2.91	1.58	5.49	3.73	6.30	0.63	0.61	524.00	0.21	0.03	0.01
	5–7	2.26	0.09	0.49	19.00	3.67	0.72	3.96	4.45	4.59	0.60	0.42	651.00	0.17	0.02	0.01
	5–8	1.79	0.07	0.46	19.40	3.81	0.86	7.46	18.60	15.40	0.83	0.84	396.00	0.58	0.04	0.01
	5–9	2.52	0.15	0.63	23.60	4.41	0.46	3.71	2.63	4.30	0.94	0.33	551.00	0.18	0.02	0.01
	5–10	4.99	0.21	0.97	24.00	5.14	0.66	5.59	6.96	4.69	1.62	0.52	438.00	0.57	0.02	0.01
	5–11	5.50	0.20	1.20	40.20	7.68	0.63	5.03	2.78	4.30	2.81	0.58	470.00	0.19	0.03	0.02
	5–12	1.64	0.17	0.48	35.80	5.74	0.62	7.02	16.20	9.43	1.15	0.39	465.00	0.15	0.03	0.01
	5–13	0.92	0.09	0.34	51.40	5.90	1.13	7.70	2.05	2.25	0.73	0.52	442.00	0.24	0.01	0.01
	5–14	0.63	0.06	0.31	32.40	4.70	2.75	6.24	1.98	2.53	0.44	0.29	454.00	0.46	0.01	0.01
	5–15	1.02	0.27	0.39	29.30	3.58	8.51	8.21	2.29	2.03	0.63	0.31	388.00	0.79	0.01	0.01
	5–16	4.11	2.03	0.62	26.30	4.15	9.40	10.60	2.75	7.47	1.54	2.79	368.00	0.93	0.02	0.01
6-2z	6z-1	2.61	4.80	1.82	35.10	5.90	6.55	6.77	18.90	15.10	2.10	0.47	581.00	0.30	0.02	0.01
	6z-2	4.00	1.37	1.01	38.90	5.60	5.22	5.98	5.67	6.30	2.24	0.36	600.00	0.11	0.02	0.01
	6z-3	1.28	0.13	0.36	33.80	4.45	5.68	11.40	19.40	23.50	1.01	0.78	557.00	0.50	0.08	0.01
	6z-4	0.83	0.08	0.25	23.00	2.68	7.25	10.00	17.70	13.20	0.85	0.31	454.00	1.24	0.06	0.01
	6z-5	1.93	0.11	0.40	38.00	3.20	3.95	9.27	4.26	4.50	0.78	0.35	559.00	0.28	0.04	0.01
	6z-6	1.84	0.14	0.34	27.20	3.65	2.54	4.54	2.97	4.45	0.48	0.69	607.00	0.35	0.03	0.01
	6z-7	1.09	0.08	0.37	24.50	3.61	6.68	7.82	2.66	4.25	0.57	0.33	535.00	0.41	0.03	0.01
	6z-8	1.32	0.10	0.36	59.30	4.53	8.19	10.40	17.50	11.30	0.79	0.24	489.00	0.90	0.10	0.01
	6z-9	0.72	0.27	0.23	21.40	2.50	7.56	7.13	16.50	10.10	0.53	0.26	449.00	1.17	0.05	0.01
	6z-10	1.87	6.77	1.03	87.00	5.64	8.08	20.30	19.80	11.80	9.42	0.33	629.00	2.47	0.03	0.01
6-2x	6x-1	3.02	2.95	2.61	37.30	6.33	7.07	5.23	3.24	17.70	7.13	0.44	585.00	344.00	1.43	0.02
	6x-2	2.76	1.55	0.62	14.30	3.51	5.35	5.06	1.75	6.43	2.80	0.26	596.00	15.40	0.09	0.01
	6x-3	3.60	0.45	0.48	33.20	4.63	5.15	4.86	2.34	7.77	1.11	0.40	712.00	2.88	0.05	0.01
	6x-4	3.37	0.27	0.59	22.00	3.28	6.54	5.09	2.06	10.30	2.02	0.33	614.00	2.75	0.06	0.01
	6x-5	2.63	0.35	0.62	43.50	4.49	9.41	7.82	6.82	7.58	3.48	0.39	739.00	5.54	0.04	0.01
	6x-6	5.58	0.99	0.98	25.30	3.59	5.92	5.74	2.38	3.56	3.94	0.58	668.00	1.10	0.02	0.01
	6x-7	6.40	0.82	0.78	55.70	6.27	8.80	15.90	16.70	29.20	9.75	1.06	959.00	2.51	0.07	0.03
	6x-8	7.81	0.71	1.66	42.00	6.05	11.30	13.00	18.50	24.40	6.57	0.74	884.00	1.04	0.06	0.02
	6x-9	6.71	0.76	1.43	27.90	4.87	14.80	12.30	5.05	22.90	16.90	0.76	913.00	1.84	0.03	0.02
	6x-10	23.20	8.21	12.00	76.00	48.30	34.50	154.00	9.76	15.10	9.56	3.38	854.00	2.00	0.11	0.04
	GM	31.80	2.11	1.68	35.10	15.40	7.08	13.70	17.50	41.40	6.55	9.25	140.00	3.08	0.25	0.05
	GWA	4.15	1.42	4.38	46.53	9.32	5.52	11.10	11.34	9.82	3.77	1.75	525.78	6.83	0.06	0.02

Coal seam	Sample	Sb	Cs	Ba	W	Re	Tl	Pb	Bi	Th	U	Nb	Ta	Zr	Hf
2–1	2–1	0.25	0.10	32.10	0.83	0.002	0.03	10.80	0.14	5.18	1.11	3.60	0.31	25.50	0.71
	2–2	0.31	0.10	28.90	1.19	0.003	0.08	6.92	0.16	7.44	1.37	4.93	0.43	41.90	1.04
3–1	3–1	0.34	0.11	35.90	1.29	0.003	0.02	6.44	0.11	6.13	2.93	6.11	0.52	52.50	1.53
	3–2	0.37	0.04	12.90	0.83	0.002	0.18	3.35	0.05	0.44	0.24	0.60	0.05	3.37	0.10
	3–3	0.09	0.04	21.00	0.60	0.003	0.01	1.22	0.05	1.69	0.24	1.07	0.11	11.60	0.28
	3–4	0.18	0.03	24.70	0.83	0.002	0.01	2.20	0.08	0.65	0.36	0.67	0.05	4.84	0.14
	3–5	0.19	0.08	47.50	0.79	0.003	0.02	5.97	0.07	1.60	0.52	1.17	0.11	10.60	0.32
	3–6	0.12	0.07	42.80	1.80	0.002	0.01	1.73	0.04	0.60	0.24	0.65	0.06	5.33	0.15

(*continued on next page*)

Table 2 (*continued*)

Coal seam	Sample	Sb	Cs	Ba	W	Re	Tl	Pb	Bi	Th	U	Nb	Ta	Zr	Hf
	3–7	0.08	0.06	36.10	0.61	<0.002	0.01	1.57	0.03	0.54	0.22	0.61	0.05	4.75	0.14
	3–8	0.11	0.12	65.10	1.22	0.002	0.34	7.33	0.09	1.21	0.78	1.09	0.09	15.20	0.34
	3–9	0.42	0.23	80.40	2.03	0.002	0.04	20.50	0.15	17.70	6.90	16.60	1.37	124.00	3.39
	3–10	0.10	0.08	41.00	0.83	<0.002	0.13	7.84	0.08	4.49	1.38	5.56	0.44	53.40	1.39
	3–11	0.10	0.05	29.10	0.63	0.002	0.43	1.66	0.04	1.37	0.51	1.70	0.14	16.40	0.45
	3–12	0.14	0.06	16.00	0.78	<0.002	0.01	1.12	0.03	1.08	0.41	1.03	0.08	7.96	0.21
	3–13	0.20	0.03	21.90	0.83	0.002	0.01	0.90	0.09	1.67	0.71	1.33	0.11	15.70	0.44
	3–14	0.12	0.04	28.20	1.16	<0.002	0.02	2.31	0.04	1.12	0.28	0.58	0.06	4.32	0.15
	3–15	8.93	0.15	14.20	2.36	<0.002	0.06	7.29	0.11	1.61	0.76	0.87	0.07	11.80	0.37
4–1	4–1	13.10	0.13	14.30	5.17	0.002	0.11	1.88	0.02	0.35	1.39	0.32	0.04	2.66	0.11
	4–2	1.28	4.35	101.00	0.94	0.002	0.29	11.20	0.39	8.08	3.54	11.00	0.59	86.20	2.11
	4–3	0.26	0.32	23.60	0.96	0.002	0.04	1.95	0.06	1.41	0.62	1.79	0.14	14.80	0.43
	4–4	0.17	0.12	21.50	0.95	<0.002	0.14	4.99	0.07	2.78	1.11	3.05	0.27	27.70	0.75
	4–5	0.17	0.09	24.40	0.53	<0.002	0.02	4.25	0.06	1.27	0.61	0.99	0.09	8.95	0.27
	4–6	2.45	5.91	92.60	1.67	0.002	0.24	5.65	0.32	7.93	3.75	9.34	0.29	35.70	1.03
	4–7	0.27	0.11	21.60	2.36	0.002	0.02	3.53	0.05	0.99	0.51	0.76	0.07	6.70	0.21
	4–8	0.20	0.22	18.90	1.68	0.002	0.02	5.19	0.06	0.76	0.30	0.73	0.06	5.59	0.17
	4–9	0.48	0.22	44.20	1.17	0.002	0.02	3.90	0.12	9.90	0.65	3.18	0.12	10.20	0.33
5–1	5–1	2.06	0.05	7.55	0.98	0.002	0.06	4.38	0.04	0.88	2.46	1.60	0.07	7.28	0.29
	5–2	0.29	1.18	33.00	0.83	<0.002	0.06	1.92	0.19	3.63	1.03	2.72	0.22	27.30	0.78
	5–3	0.21	0.09	8.89	1.17	<0.002	0.04	2.43	0.03	0.35	0.17	0.42	0.03	2.64	0.10
	5–4	0.21	0.04	31.20	0.33	<0.002	0.01	3.42	0.07	8.87	0.32	2.27	0.07	4.40	0.14
	5–5	0.05	0.03	18.10	0.26	0.002	0.03	1.50	0.03	0.99	0.20	1.02	0.10	7.11	0.20
	5–6	0.08	0.05	12.10	0.38	<0.002	0.01	4.46	0.03	0.77	0.32	0.68	0.06	6.79	0.20
	5–7	0.06	0.03	10.10	0.26	<0.002	0.00	1.62	0.04	1.07	0.28	1.12	0.11	12.90	0.35
	5–8	0.37	0.08	19.10	0.40	0.002	0.01	2.56	0.04	0.51	0.35	0.59	0.05	3.91	0.12
	5–9	0.06	0.03	8.00	0.30	<0.002	0.00	1.25	0.06	1.33	0.39	1.35	0.11	16.10	0.29
	5–10	0.11	0.05	8.06	0.34	<0.002	0.01	1.87	0.06	1.50	0.63	1.54	0.13	12.30	0.36
	5–11	0.15	0.05	7.00	0.39	<0.002	0.01	2.09	0.07	1.88	1.15	2.73	0.15	24.10	0.73
	5–12	0.11	0.03	12.30	0.34	<0.002	0.00	2.12	0.04	1.13	0.49	1.17	0.09	9.98	0.30
	5–13	0.06	0.03	5.66	0.45	<0.002	0.01	0.96	0.05	0.63	0.26	0.69	0.06	5.31	0.16
	5–14	0.06	0.03	7.04	0.37	<0.002	0.10	1.69	0.04	0.48	0.15	0.52	0.04	3.79	0.12
	5–15	0.06	0.05	6.14	0.67	<0.002	0.10	2.28	0.02	0.37	0.11	0.31	0.03	2.47	0.07
	5–16	0.09	0.10	11.90	3.25	<0.002	0.03	14.50	0.08	8.62	0.90	8.19	0.87	21.40	0.66
6-2z	6z-1	0.27	0.03	17.70	0.41	<0.002	0.00	1.50	0.06	1.08	0.56	0.84	0.08	8.78	0.27
	6z-2	0.09	0.03	8.50	0.32	0.002	0.00	0.63	0.09	3.15	0.47	1.73	0.20	39.30	0.92
	6z-3	0.29	0.05	23.20	0.58	<0.002	0.05	4.93	0.07	2.29	0.58	1.02	0.06	4.95	0.15
	6z-4	0.23	0.03	16.10	0.58	<0.002	0.28	6.30	0.04	1.57	0.20	0.56	0.03	2.75	0.08
	6z-5	0.10	0.04	14.90	0.40	<0.002	0.01	0.99	0.05	0.95	0.41	1.16	0.10	8.39	0.23
	6z-6	0.07	0.06	16.00	0.23	<0.002	0.01	4.22	0.05	0.78	0.33	0.49	0.06	5.09	0.15
	6z-7	0.10	0.02	11.50	0.54	<0.002	0.00	1.24	0.04	0.59	0.25	0.40	0.03	3.33	0.10
	6z-8	0.12	0.02	14.40	0.54	<0.002	0.04	2.31	0.05	0.54	0.18	0.52	0.05	4.67	0.15
	6z-9	0.11	0.02	13.20	0.35	<0.002	0.01	1.35	0.03	0.36	0.18	0.31	0.03	2.89	0.09
	6z-10	0.77	0.03	15.40	1.02	0.002	0.04	2.97	0.08	0.55	0.88	0.36	0.04	2.95	0.13
6-2x	6x-1	0.30	0.03	10.40	0.44	0.002	0.31	5.33	0.08	1.54	1.57	2.22	0.15	15.00	0.43
	6x-2	0.07	0.02	16.70	0.20	<0.002	0.03	1.14	0.05	0.93	0.51	0.73	0.07	6.98	0.21
	6x-3	0.07	0.03	13.20	0.19	<0.002	0.01	1.49	0.06	0.84	0.38	0.65	0.05	4.81	0.16
	6x-4	0.08	0.03	30.70	0.24	<0.002	0.00	1.16	0.05	0.69	0.47	0.73	0.05	6.05	0.15
	6x-5	0.12	0.04	249.00	0.56	<0.002	0.02	2.94	0.05	0.87	0.49	0.90	0.08	7.99	0.24
	6x-6	0.15	0.08	94.20	0.18	<0.002	0.01	5.17	0.07	0.82	1.98	0.54	0.06	7.65	0.24
	6x-7	0.39	0.05	153.00	0.49	0.002	0.01	8.37	0.06	3.10	1.83	3.15	0.32	12.60	0.41
	6x-8	0.35	0.03	92.70	0.29	<0.002	0.01	5.44	0.08	2.92	0.75	2.86	0.27	13.90	0.43
	6x-9	1.25	0.04	136.00	0.54	<0.002	0.01	10.10	0.10	2.45	3.54	2.95	0.18	8.60	0.33
	6x-10	1.66	0.36	30.40	0.65	<0.002	0.40	58.70	0.28	12.80	2.32	7.45	0.83	68.70	2.07
	GM	0.66	0.25	34.44	0.86	<0.002	0.07	4.95	0.08	2.58	0.94	2.19	0.17	16.30	0.46
	GWA	0.84	1.13	159.00	1.08	——	0.47	15.10	0.79	5.84	2.43	9.44	0.62	89.50	3.71

GM: Geometric average content CWA: Average values for China coals (Dai et al., 2012)

3. Sampling and analytical methods

The coal samples were from the Gaoxigou and Nayuan coal mines (Fig. 1B). Sixty-two coal samples were collected from different levels in the Dongsheng area (Fig. 1C). Each sample was cut into small cubes with dimensions of 5 cm × 5 cm × 5 cm at 0.25-m intervals. All samples were immediately stored in plastic bags to minimize contamination and oxidation in the field. In the lab, all samples were crushed to 200 mesh for the chemical analyses.

All samples were subjected to elemental geochemical analysis in the laboratory of the Analysis and Testing Research Center of the Beijing Geological Research Institute of Nuclear Industry. The analysis was performed using the test method proposed by Kimura (1998). The processed 200-mesh powder sample was placed in a 35-mm-diameter PVC plastic mold with a boric acid bottom and then pressed under a pressure of 25 tons. The sample was completely digested using the sample digestion method proposed by Liu (1996). For every 50 (±1) mg of sample to be digested, 2 ml of concentrated nitric acid (HNO_3) and 1 ml of hydrofluoric acid (HF) should be added. The X-ray fluorescence spectrometry (XRF) were used to determine the content of major-element oxides (SiO_2, $A1_2O_3$, CaO, K_2O, Na_2O, Fe_2O_3, MnO, MgO, TiO_2, and P_2O_5). The trace and rare earth elements were determined using Inductively-coupled plasma mass spectrometer (ICP-MS).

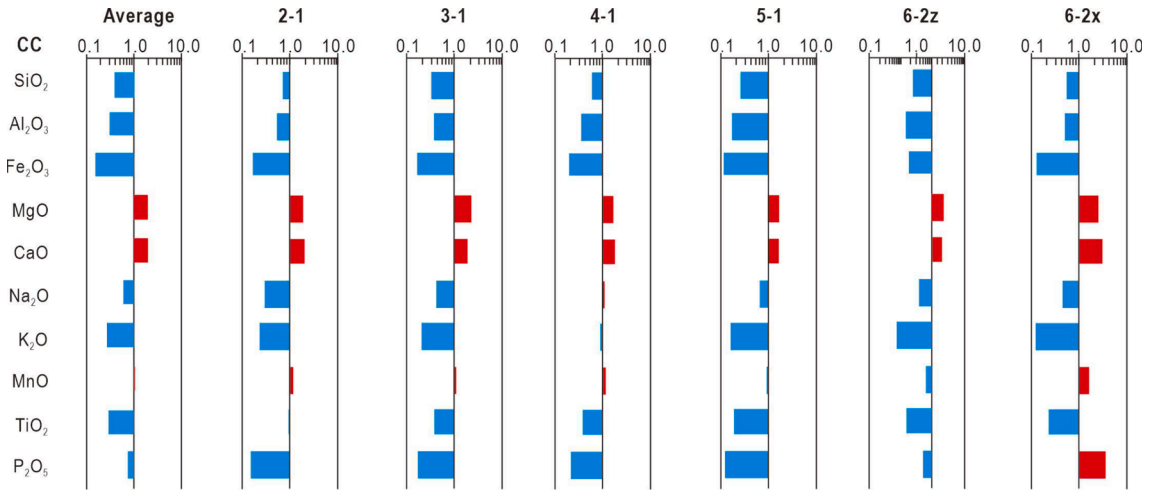

Fig. 2. Concentration coefficients (CC) of major elements in the Yan'an coals. Normalized to average for Chinese coals (Dai et al., 2012).

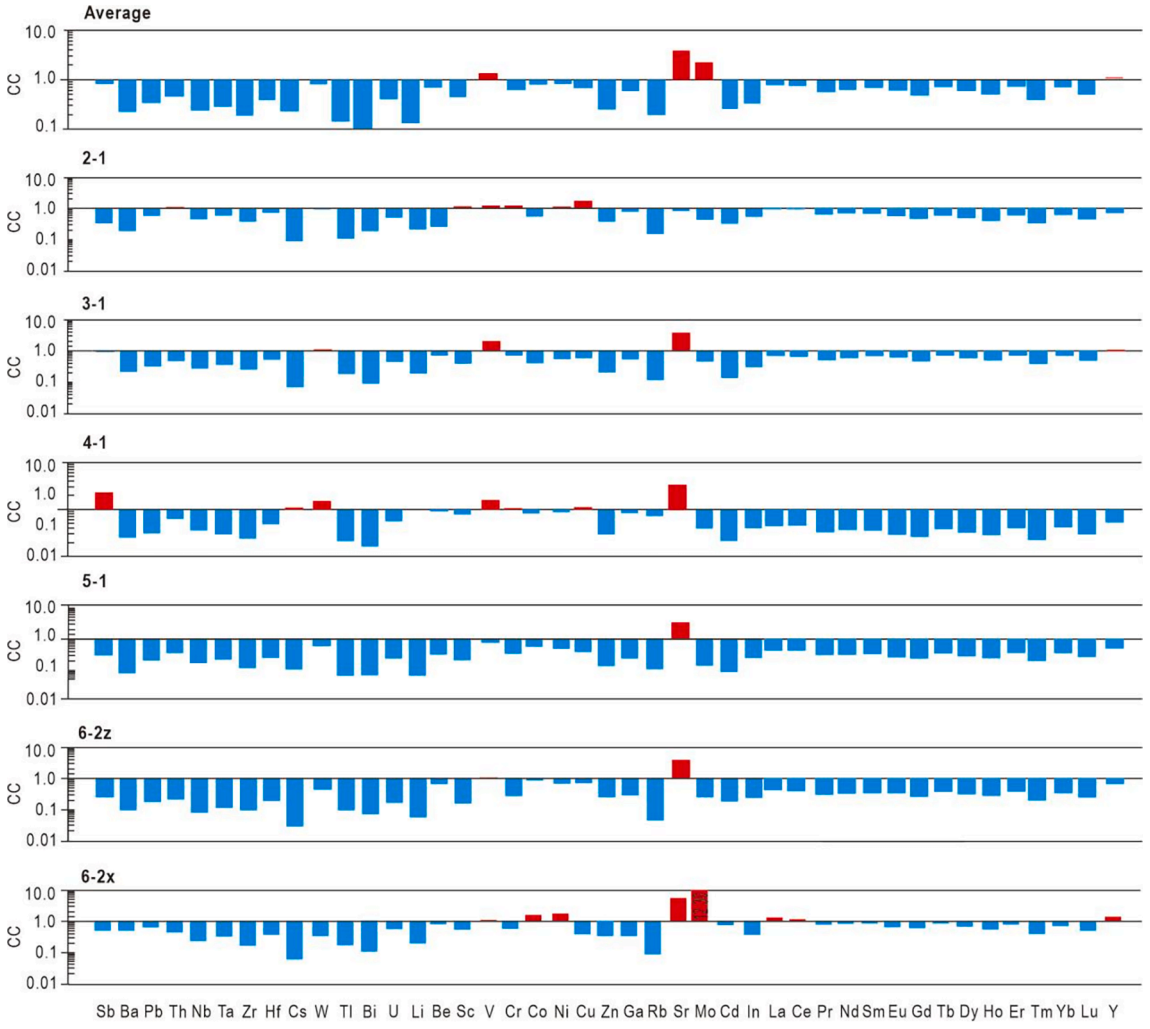

Fig. 3. Concentration coefficients (CC) of trace elements in the Yan'an coals. Normalized to average for Chinese coals (Dai et al., 2012).

4. Results

4.1. Major elements

The major element oxides in Yan'an Formation coal are SiO_2 and CaO. The remaining major element oxides have values lower than the corresponding averages for Chinese coals (Table 1). This result is similar to the result obtained by Wang et al. (2011) from Jurassic coals in the Dongsheng area of the Ordos Basin. The major elements, mainly Na_2O, MnO, and P_2O_5, are enriched ($5 < CC < 10$, CC = ratio of element

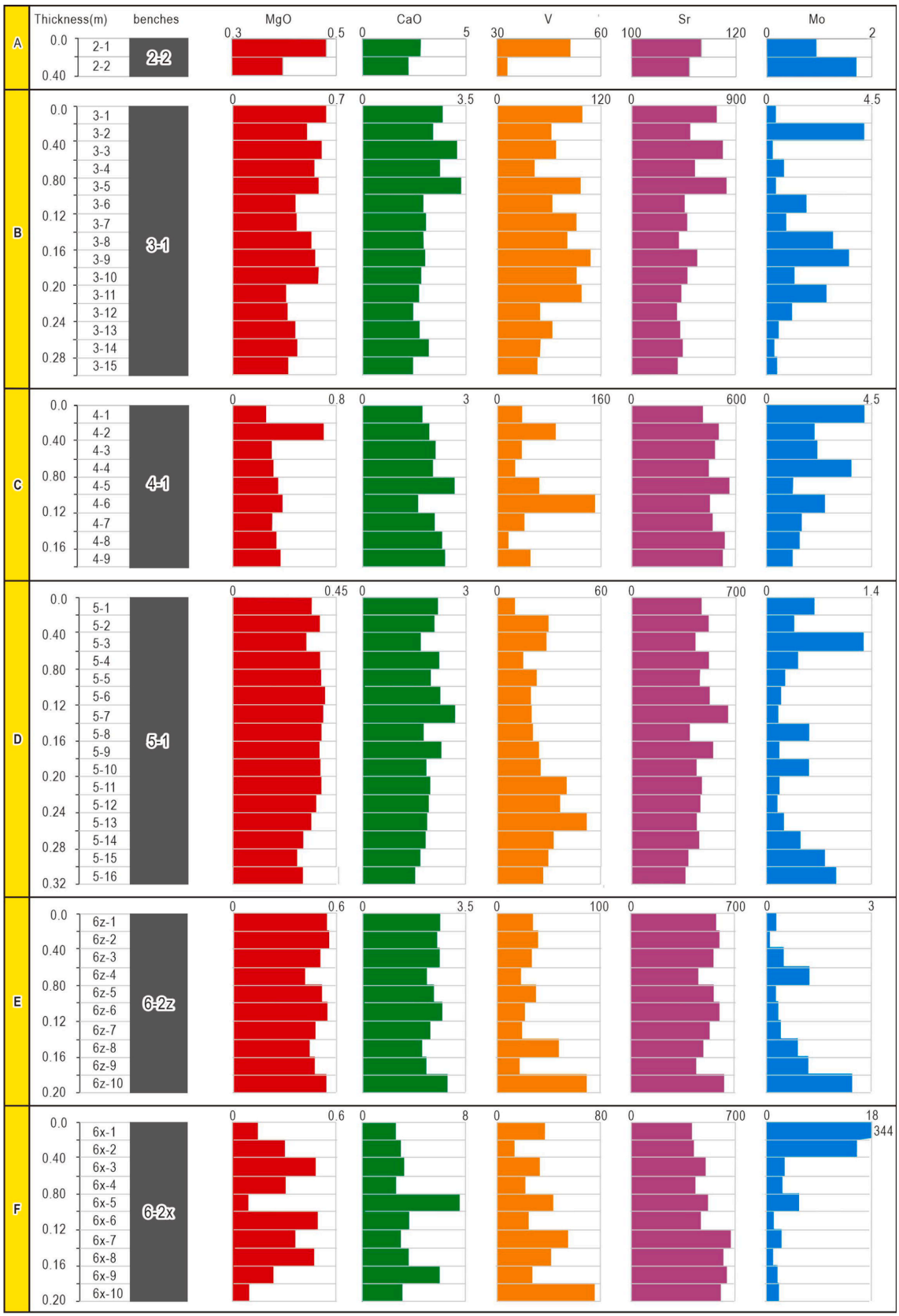

Fig. 4. Variations of MgO, CaO, V, Sr and Mo (μg/g) in Yan'an Formation.

Table 3
Yttrium and rare earth elements of coal samples in Yan'an Formation (μg/g).

Coal seam	Sample	La	Ce	Pr	Nd	Sm	Eu	Gd	Tb	Dy	Y	Ho	Er	Tm	Yb	Lu
2–1	2–1	10.80	22.70	2.32	8.56	1.34	0.26	1.28	0.19	1.05	6.39	0.21	0.57	0.10	0.61	0.09
	2–2	11.00	22.00	2.34	8.47	1.42	0.29	1.28	0.20	1.05	5.81	0.23	0.57	0.11	0.67	0.10
3–1	3–1	19.60	35.60	4.17	17.00	3.66	0.89	3.41	0.71	4.21	30.80	0.98	2.48	0.47	2.71	0.39
	3–2	3.59	6.55	0.79	3.36	0.75	0.20	0.78	0.15	0.92	9.61	0.23	0.55	0.10	0.48	0.07
	3–3	4.25	7.30	0.79	3.52	0.51	0.09	0.52	0.08	0.37	4.15	0.08	0.21	0.04	0.21	0.03
	3–4	3.68	6.43	0.69	2.65	0.42	0.08	0.43	0.05	0.28	2.15	0.06	0.15	0.03	0.16	0.02
	3–5	3.55	5.95	0.59	2.23	0.37	0.06	0.34	0.06	0.30	1.74	0.06	0.16	0.03	0.19	0.03
	3–6	2.32	4.02	0.44	1.76	0.34	0.07	0.30	0.05	0.26	1.57	0.06	0.15	0.03	0.16	0.02
	3–7	2.11	3.13	0.35	1.31	0.22	0.05	0.20	0.03	0.18	0.95	0.04	0.09	0.02	0.11	0.02
	3–8	2.84	5.43	0.60	2.45	0.44	0.08	0.39	0.06	0.33	2.00	0.08	0.20	0.04	0.26	0.04
	3–9	49.00	98.20	11.70	47.10	8.98	1.65	7.81	1.28	6.50	27.90	1.24	2.95	0.54	3.26	0.45
	3–10	9.03	17.20	1.77	6.52	1.15	0.23	1.09	0.18	0.94	4.69	0.20	0.51	0.10	0.62	0.08
	3–11	4.69	7.48	0.84	2.86	0.51	0.09	0.46	0.07	0.37	1.96	0.08	0.22	0.04	0.28	0.04
	3–12	3.50	6.15	0.67	2.34	0.36	0.06	0.35	0.05	0.25	1.34	0.05	0.14	0.02	0.17	0.02
	3–13	3.35	5.97	0.67	2.42	0.34	0.05	0.33	0.05	0.25	1.41	0.05	0.12	0.02	0.12	0.02
	3–14	6.32	15.00	1.94	8.14	1.77	0.43	1.70	0.33	1.81	15.70	0.38	0.92	0.14	0.71	0.09
	3–15	4.77	11.00	1.65	7.60	2.13	0.60	2.06	0.50	2.95	21.30	0.72	1.72	0.30	1.82	0.25
4–1	4–1	2.81	6.69	1.02	4.95	1.62	0.45	1.56	0.43	2.77	18.30	0.69	1.80	0.36	2.11	0.30
	4–2	17.40	36.90	4.43	16.90	3.50	0.75	3.09	0.57	3.03	20.10	0.71	1.79	0.34	2.11	0.27
	4–3	5.87	12.50	1.59	6.61	1.46	0.32	1.42	0.27	1.47	12.40	0.34	0.75	0.13	0.73	0.10
	4–4	8.95	17.00	1.91	7.46	1.23	0.20	1.17	0.17	0.79	5.56	0.17	0.44	0.08	0.51	0.07
	4–5	5.17	10.20	1.19	4.66	1.02	0.24	0.95	0.18	1.06	8.88	0.25	0.64	0.12	0.70	0.10
	4–6	29.60	70.20	7.68	29.10	5.24	1.12	4.77	0.87	4.72	24.40	1.03	2.62	0.50	2.90	0.43
	4–7	4.19	9.14	1.11	5.01	1.07	0.28	1.08	0.23	1.40	12.00	0.36	0.94	0.19	1.17	0.16
	4–8	4.69	10.10	1.20	5.04	0.98	0.27	1.04	0.19	1.09	10.90	0.26	0.63	0.11	0.58	0.08
	4–9	23.70	53.60	6.07	21.00	2.77	0.58	3.08	0.41	1.86	11.90	0.34	0.86	0.13	0.69	0.10
5–1	5–1	4.32	11.00	1.39	6.39	1.79	0.50	1.92	0.51	3.47	26.60	0.91	2.14	0.44	2.65	0.39
	5–2	8.00	18.40	2.04	8.06	1.63	0.36	1.48	0.28	1.50	11.90	0.36	0.86	0.15	0.93	0.13
	5–3	2.46	5.38	0.63	2.57	0.51	0.10	0.43	0.08	0.41	2.99	0.09	0.21	0.04	0.23	0.03
	5–4	20.70	47.80	5.52	17.40	1.85	0.32	2.18	0.22	0.86	2.27	0.11	0.32	0.03	0.17	0.02
	5–5	1.94	3.63	0.40	1.52	0.26	0.05	0.26	0.05	0.26	1.52	0.06	0.14	0.03	0.15	0.02
	5–6	2.17	3.91	0.44	1.62	0.27	0.05	0.26	0.04	0.23	1.38	0.05	0.13	0.03	0.15	0.02
	5–7	2.41	4.20	0.46	1.66	0.29	0.06	0.26	0.04	0.25	1.45	0.06	0.15	0.03	0.19	0.03
	5–8	1.98	3.90	0.47	1.72	0.31	0.06	0.29	0.05	0.23	1.30	0.05	0.13	0.03	0.14	0.02
	5–9	3.16	5.96	0.72	2.49	0.43	0.08	0.39	0.06	0.30	1.55	0.06	0.16	0.03	0.21	0.03
	5–10	4.25	8.57	0.96	3.36	0.56	0.10	0.53	0.08	0.43	2.26	0.09	0.24	0.04	0.26	0.04
	5–11	4.00	8.78	0.98	3.54	0.65	0.09	0.53	0.09	0.50	2.48	0.10	0.27	0.06	0.37	0.05
	5–12	4.15	8.04	1.00	3.49	0.62	0.10	0.51	0.08	0.39	2.03	0.09	0.23	0.05	0.30	0.04
	5–13	2.68	4.92	0.57	2.08	0.35	0.06	0.29	0.05	0.23	1.45	0.05	0.12	0.02	0.15	0.02
	5–14	1.89	3.04	0.33	1.16	0.17	0.03	0.17	0.03	0.13	0.77	0.03	0.07	0.01	0.09	0.01
	5–15	2.85	4.76	0.48	1.74	0.24	0.05	0.27	0.04	0.18	1.43	0.04	0.08	0.01	0.09	0.01
	5–16	12.30	23.80	2.39	8.15	1.49	0.19	1.49	0.27	1.47	9.77	0.33	0.75	0.12	0.61	0.08
6-2z	6z-1	10.20	20.90	2.35	8.44	1.52	0.37	1.60	0.29	1.66	15.10	0.41	0.98	0.20	1.07	0.16
	6z-2	2.61	5.63	0.70	2.92	0.64	0.15	0.61	0.11	0.64	6.54	0.16	0.39	0.07	0.38	0.05
	6z-3	7.39	16.30	1.82	6.58	0.86	0.15	0.89	0.12	0.52	3.23	0.09	0.24	0.03	0.21	0.03
	6z-4	6.86	14.50	1.62	5.60	0.73	0.14	0.78	0.10	0.42	2.25	0.07	0.17	0.02	0.13	0.02
	6z-5	3.50	4.49	0.48	1.62	0.27	0.05	0.24	0.04	0.20	1.21	0.05	0.11	0.02	0.13	0.02
	6z-6	2.98	3.99	0.40	1.37	0.18	0.04	0.22	0.03	0.18	1.07	0.04	0.11	0.02	0.13	0.02
	6z-7	2.78	4.11	0.44	1.51	0.23	0.05	0.23	0.03	0.20	1.08	0.04	0.10	0.02	0.13	0.02
	6z-8	1.66	2.88	0.33	1.20	0.21	0.05	0.20	0.03	0.17	1.26	0.04	0.10	0.02	0.12	0.02
	6z-9	2.05	3.57	0.42	1.53	0.26	0.05	0.25	0.04	0.19	1.60	0.04	0.09	0.02	0.10	0.01
	6z-10	8.46	17.10	2.34	9.68	2.16	0.62	2.19	0.45	2.54	25.30	0.62	1.36	0.21	1.10	0.16
6-2x	6x-1	3.70	8.91	1.06	4.75	1.09	0.28	1.14	0.27	1.71	16.30	0.44	1.13	0.21	1.24	0.18
	6x-2	2.77	6.63	0.82	3.51	0.81	0.18	0.79	0.18	1.05	10.40	0.25	0.62	0.12	0.62	0.09
	6x-3	4.02	7.23	0.82	3.19	0.63	0.11	0.57	0.11	0.58	5.79	0.13	0.32	0.06	0.33	0.04
	6x-4	11.80	15.00	1.23	3.67	0.58	0.09	0.67	0.09	0.49	4.23	0.11	0.29	0.05	0.33	0.05
	6x-5	18.90	28.10	2.80	9.56	1.38	0.17	1.28	0.18	0.84	4.85	0.16	0.42	0.07	0.42	0.06
	6x-6	2.01	5.49	0.81	3.38	0.87	0.13	0.64	0.13	0.74	4.76	0.17	0.45	0.09	0.59	0.09
	6x-7	56.10	86.40	7.96	21.90	2.49	0.31	3.22	0.34	1.67	7.08	0.27	0.77	0.12	0.78	0.11
	6x-8	9.12	19.60	2.19	7.91	1.38	0.21	1.27	0.21	1.06	7.93	0.22	0.55	0.10	0.60	0.08
	6x-9	27.20	68.80	9.35	40.70	8.13	1.52	6.76	1.14	5.24	44.80	1.01	2.32	0.29	1.57	0.19
	6x-10	9.03	22.40	2.46	9.32	2.21	0.42	1.92	0.43	2.49	16.40	0.56	1.32	0.25	1.43	0.21
	UCC	16.00	33.00	3.90	16.00	3.50	1.10	3.30	0.60	3.70	20.00	0.78	2.20	0.32	2.20	0.30

UCC: Upper Continental Crust (Taylor and McLennan, 1985).

concentration in investigated coals vs. averages for Chinese coals); CaO and MgO are slightly enriched (2 < CC < 5) compared to the average for Chinese coals (Dai et al., 2012); and SiO_2, Fe_2O_3, $A1_2O_3$, K_2O, and TiO_2 are depleted (CC < 0.5).

4.2. Trace elements

The trace contents in the coal of the Yan'an Formation are listed in Table 2. Compared with the average values for Chinese coals (Dai et al., 2012), only Sr and Mo are slightly enriched (2 < CC < 5). The highest enrichment element is Sr, with a value of 3.76. The concentrations of the remaining trace elements are close to the average values for Chinese coals (0.5 < CC < 2), the enrichment coefficient of V element is 1.33 (Fig. 3, A). Thus, the contents of Sr, Mo, and V in each layer have been studied (Fig. 4), showing that the contents of Mo and V in each layer did not have significant variation. However, the content of Sr decreased

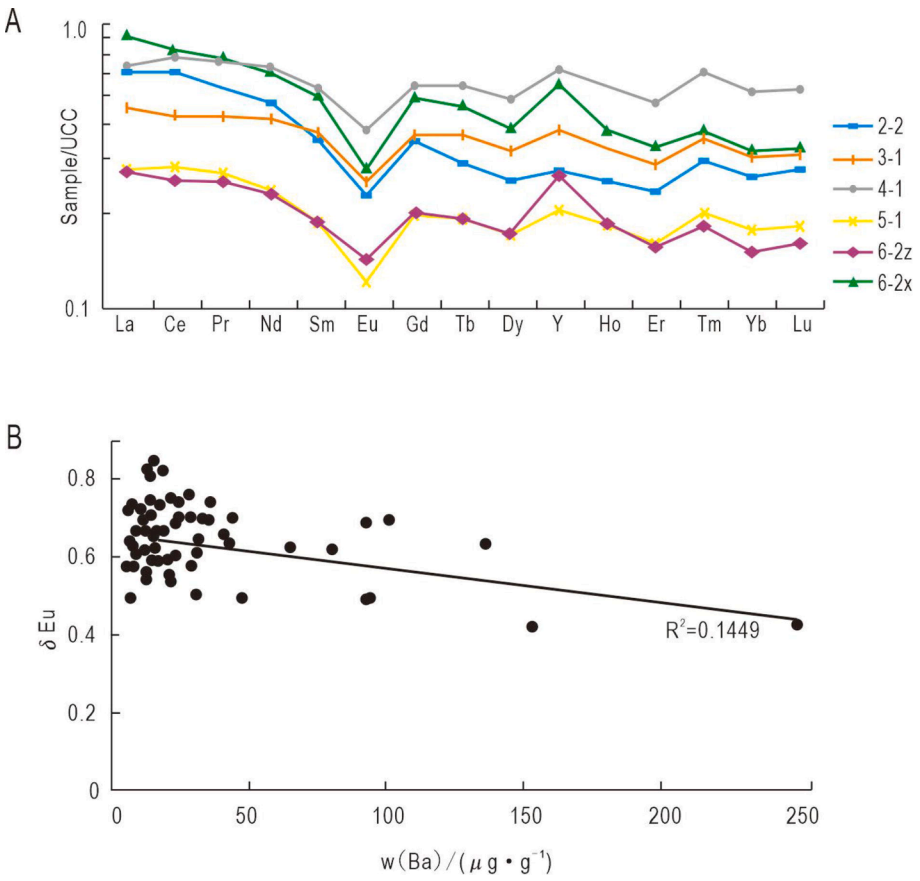

Fig. 5. Distribution patterns of REY in the samples. (A) REY are normalized by Upper Continental Crust (UCC) (Taylor and McLennan, 1985). (B) Diagram of the relationship between δ Eu and ω(Ba) of samples.

during coal deposition.

5. Discussion

5.1. Geochemical characteristics

The major element oxides representing the terrestrial clastic material components in coal are SiO_2, as seen in the quartz (Han, 1996). Because most of the quartz in coal is terrigenous, carried by geological forces such as water or wind into peat bogs and preserved in coal seams. The content of major elements in the coal seams in the study area is dominated by SiO_2, which indicates that the material source may be mainly terrigenous debris. Huang et al. (2009) also found that the whole basin had a stable deposition provenance in the late Paleozoic.

Each layer is summarized and compared with the enrichment coefficients (Fig. 2B-G). CaO and MgO are slightly enriched in every layer. However, the enrichment coefficient in the 6-2x coal is higher, which is shown as mild enrichment. Compared to the other coal seams, only P_2O_5 in the 6-2x coal seam is slightly concentrated. Meanwhile, the content of CaO and MgO with high concentration elements in each layer was studied (Fig. 4). It can be concluded that the contents of CaO and MgO contents in each layer have no noticeable change (Fig. 4). However, the contents of CaO and MgO in the 6-2x coal seam are relatively unstable (Fig. 4).

The enrichment characteristics of coal trace elements (Fig. 3, B-G) demonstrated that the V content at the top of the coal seam is slightly higher than at the bottom. It indicates that the enrichment coefficient of elements Th, Sc, V, Cr, Ni, and Cu is high in the 2–1 coal seam and the enrichment coefficient of Sr element is low. However, the Sr element enrichment coefficient in the coal seams except the 2–1 coal seam is high (Fig. 3, B-G).

Wang et al. (2018) also found that most trace elements in coals of the Yan'an Formation are depleted. The concentration is close to the corresponding average of the world's low coal grade coal. This is also consistent with our conclusion from this study.

Rare earth elements and Yttrium (REY) are often discussed together because of their similar geochemical properties (Seredin and Dai, 2012). Therefore, a three-fold geochemical classification of rare earth elements and Yttrium was used in this study: light (LREY: La, Ce, Pr, Nd, and Sm), medium (MREY: Eu, Gd, Tb, Dy, and Y), and heavy (HREY: Ho, Er, Tm, Yb, and Lu) REYs (Seredin and Dai, 2012).

The REY concentrations from average values for Chinese coals and their comparison with the Yan'an Formation coal samples are listed in Table 3. The concentration of REY in Yan'an coal is 7.92 ~ 268.56 μg/g (Table 3). The average concentration of total REY in Yan'an Formation coal is 48.49 μg/g, close to the average value for world low-rank coals (65.3 μg/g; Ketris and Yudovich, 2009), lower than the average value for China coals (135.89 μg/g; Dai et al., 2012). The enrichment of REY in Yan'an Coal is 0.62, and all elements except Yttrium are<1 (Fig. 3A). REY enrichment in each coal seam is relatively low, except for La, Ce, and Y in the 6-2X coal seam (Fig. 3, B-G). Europium in all the coals shows apparent negative anomalies (Fig. 5A). Dai et al. (2016) noted that Eu anomalies could be caused by the interference from BaO and/or BaOH during the ICP-MS analysis. However, the weak relation between Ba and Eu concentrations (R = 0.024; Fig. 5B) in the investigated samples suggests that the interference of Ba does not cause the Eu anomalies in Yan'an Formation coals. Excluding the interference of Ba, it is generally believed that the Eu anomaly of the source rock caused the Eu anomaly of the element in coal (Birk and White, 1991; Dai et al., 2014; Eskenazy, 1987), as shown by the strong correlation between rare earth elements in Yan'an Formation coal and land-based debris rock.

The REY concentrations in coals have been normalized to chondrite

Table 4
Geochemistry parameters of rare earth elements of coal samples in Yan'an Formation.

Coal seam	Sample	∑REY	La_N/Lu_N	La_N/Sm_N	Gd_N/Lu_N	δEu	δCe	Enrichment type
2–1	2–1	56.47	2.28	0.18	1.31	0.64	1.09	L
	2–2	55.54	2.15	0.17	1.21	0.70	1.05	L
3–1	3–1	127.07	0.93	0.12	0.79	0.74	0.92	H
	3–2	28.12	0.96	0.11	1.02	0.82	0.90	H
	3–3	22.15	2.85	0.18	1.68	0.59	0.88	L
	3–4	17.27	3.29	0.19	1.87	0.70	0.93	L
	3–5	15.65	2.38	0.21	1.11	0.49	0.93	L
	3–6	11.54	2.07	0.15	1.29	0.64	0.91	L
	3–7	8.79	2.47	0.21	1.13	0.69	0.82	L
	3–8	15.23	1.52	0.14	1.01	0.62	0.97	L
	3–9	268.56	2.03	0.12	1.57	0.62	0.98	L
	3–10	44.30	2.17	0.17	1.27	0.66	1.02	L
	3–11	19.97	2.25	0.20	1.07	0.58	0.89	L
	3–12	15.47	3.13	0.21	1.50	0.59	0.96	L
	3–13	15.16	3.49	0.21	1.67	0.54	0.95	L
	3–14	55.39	1.27	0.08	1.66	0.76	1.05	L
	3–15	59.37	0.35	0.05	0.74	0.81	0.94	H
4–1	4–1	45.85	0.18	0.04	0.48	0.74	0.92	H
	4–2	111.89	1.20	0.11	1.03	0.69	1.04	L
	4–3	45.96	1.07	0.09	1.25	0.69	0.99	L
	4–4	45.69	2.47	0.16	1.56	0.55	0.97	L
	4–5	35.37	0.99	0.11	0.88	0.74	0.99	H
	4–6	185.18	1.30	0.12	1.02	0.69	1.16	L
	4–7	38.33	0.48	0.09	0.60	0.75	0.99	H
	4–8	37.15	1.16	0.10	1.24	0.82	1.02	L
	4–9	127.08	4.63	0.19	2.92	0.70	1.14	L
5–1	5–1	64.43	0.21	0.05	0.44	0.73	1.07	H
	5–2	56.08	1.15	0.11	1.03	0.70	1.11	L
	5–3	16.16	1.54	0.11	1.32	0.61	1.04	L
	5–4	99.78	18.48	0.24	9.44	0.61	1.18	L
	5–5	10.27	1.82	0.16	1.16	0.59	0.98	L
	5–6	10.75	1.77	0.17	1.02	0.62	0.95	L
	5–7	11.54	1.81	0.18	0.95	0.67	0.94	L
	5–8	10.67	1.95	0.14	1.40	0.66	1.00	L
	5–9	15.61	2.19	0.16	1.30	0.63	0.98	L
	5–10	21.76	2.15	0.17	1.29	0.58	1.05	L
	5–11	22.49	1.56	0.14	1.00	0.49	1.11	L
	5–12	21.10	1.85	0.15	1.10	0.55	0.99	L
	5–13	13.05	2.28	0.17	1.20	0.57	0.96	L
	5–14	7.92	2.73	0.25	1.20	0.64	0.89	L
	5–15	12.27	4.11	0.26	1.87	0.72	0.93	L
	5–16	63.20	3.00	0.18	1.76	0.39	1.06	L
6-2z	6z-1	65.24	1.21	0.15	0.92	0.73	1.05	L
	6z-2	21.59	0.91	0.09	1.02	0.72	1.01	H
	6z-3	38.46	4.95	0.19	2.88	0.60	1.11	L
	6z-4	33.41	7.15	0.20	3.94	0.64	1.09	L
	6z-5	12.43	3.65	0.28	1.23	0.59	0.76	L
	6z-6	10.77	2.94	0.36	1.04	0.62	0.79	L
	6z-7	10.96	2.74	0.26	1.11	0.69	0.84	L
	6z-8	8.29	1.95	0.17	1.16	0.71	0.93	L
	6z-9	10.21	2.75	0.17	1.61	0.66	0.92	L
	6z-10	74.29	0.97	0.09	1.21	0.85	0.94	H
6-2x	6x-1	42.42	0.38	0.07	0.56	0.72	1.07	H
	6x-2	28.84	0.58	0.08	0.80	0.66	1.07	H
	6x-3	23.93	1.84	0.14	1.27	0.55	0.94	L
	6x-4	38.69	4.43	0.44	1.22	0.50	0.80	L
	6x-5	69.19	5.81	0.30	1.91	0.43	0.86	L
	6x-6	20.34	0.44	0.05	0.67	0.49	1.08	H
	6x-7	189.51	9.48	0.49	2.64	0.42	0.93	L
	6x-8	52.43	2.04	0.14	1.37	0.49	1.09	L
	6x-9	219.02	2.73	0.07	3.29	0.63	1.05	L
	6x-10	70.84	0.81	0.09	0.84	0.57	1.19	H
	Average	48.49	2.51	0.16	1.47	0.64	0.99	

Note. Alternation: $\sum REY = La + Ce + Pr + Nd + Sm + Eu + Gd + Tb + Dy + Y + Ho + Er + Tm + Yb + Lu$; $\delta Eu = Eu_N/Eu_N^* = Eu_N/[(Sm_N \times 0.67) + (Tb_N \times 0.33)]$, $\delta Ce = Ce_N/Ce_N^* = Ce_N/[(La_N \times 0.67 + Nd_N \times 0.33)]$ (Bau and Dulski, 1996); Sm_N, Eu_N, Gd_N, Tb_N, La_N, Lu_N, Ce_N, and Nd_N are the normalized ratio of rare earth elements in the Upper Continental Crust (Taylor and McLennan, 1985).

in some investigations of REY distribution patterns (Wang et al., 1997; Wang and Yang, 2008; Zhao et al., 2012). However, this is not advisable as the normalization standard should have been affected by similar fractionation processes to the samples being normalized (Dai et al., 2016). Therefore, the REY in coal is normalized to the Upper Continental Crust in this study (upper continental crust; Taylor and McLennan, 1985). The distribution patterns of REY in Yan'an Formation coal show the V-shaped pattern, indicating negative Eu anomalies (Fig. 5A). This suggests that the peat bog had a stable terrigenous material supply during the coal-forming period (Birk and White, 1991; Dai et al., 2020).

Compared with REY concentration in the UCC (upper continental crust; Taylor and McLennan, 1985), three enrichment types are

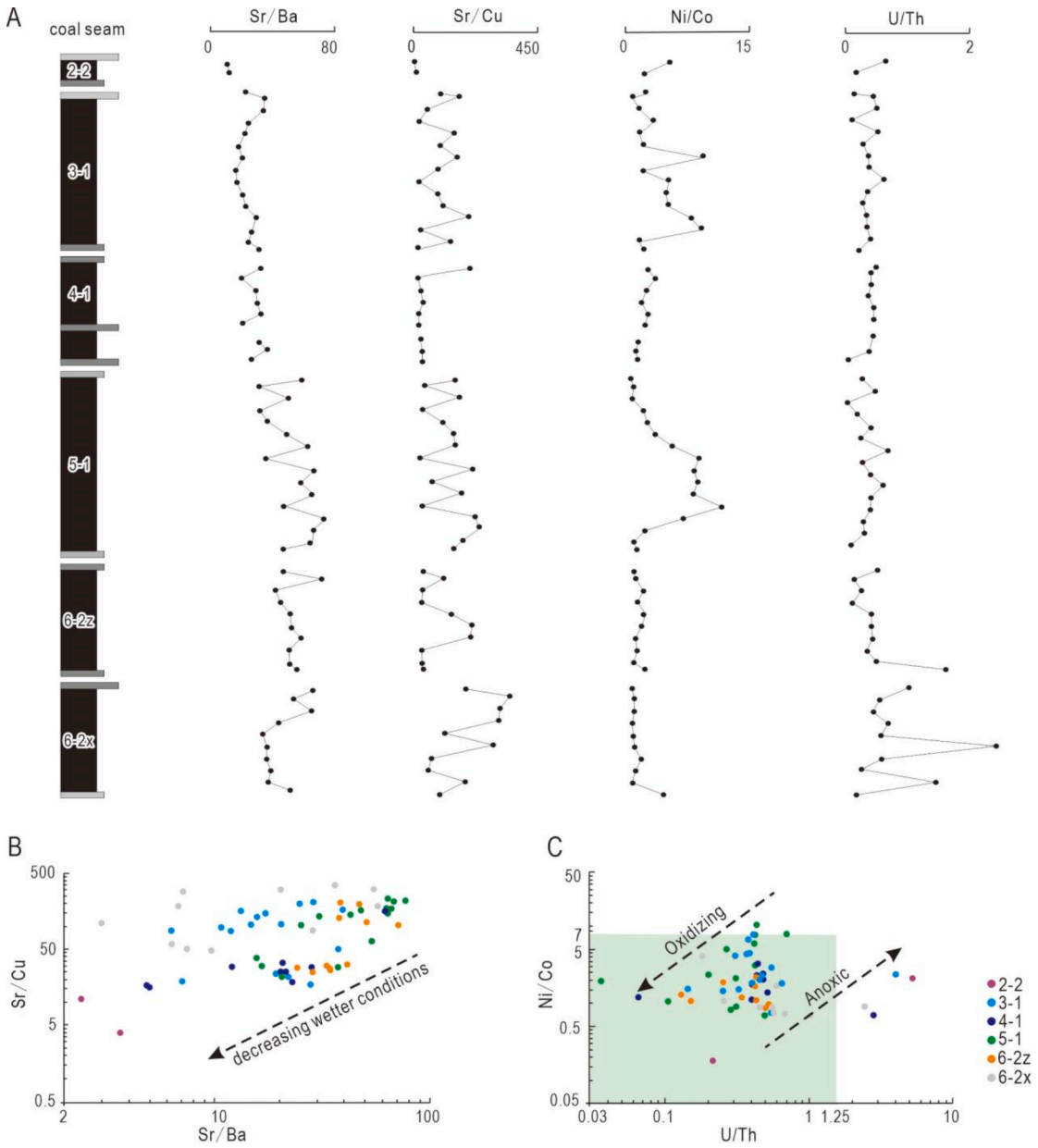

Fig. 6. Trace element ratios distributions in samples of different coal seams. (A) The Plot showing variation of the ratios calculated from the trace element composition in the samples. (B) Relationship between the Strontium/Barium (Sr/Ba) and Strontium/Copper (Sr/Cu) ratios. (C) Relationship between Nickel/Cobalt (Ni/Co) and Uranium/Thorium (U/Th) ratios.

identified: L-type ($La_N/Lu_N > 1$), M-type ($La_N/Sm_N < 1$, $Gd_N/Lu_N > 1$), and H-type ($La_N/Lu_N < 1$). The La_N/Lu_N of coal in the Yan'an Formation ranges from 0.18 to 18.48, with an average of 2.51 (Table 4). The REY in Yan'an coal are low in concentrations and characterized by the distinct L-type enrichment. The concentrations of the remaining trace elements are close to the average values for Chinese coals ($0.5 < CC < 2$). The content of rare earth elements is generally low in Yan'an Formation (Liu et al., 2007).

5.2. *The paleoenvironmental significance of peat deposition*

The environmental settings affect the trace element concentrations in sediments (Boucot and Gray, 2001; Chermak and Schreiber, 2014). In coals, trace elements and REY contain important geological information, so the occurrence state and composition of trace elements in coal have been extensively studied (Dai et al., 2015, 2016, 2017, 2018). In modern sediments, some sensitive element indicators are successfully applied to reconstruct paleoclimate (Gan et al., 2018; Mathews et al., 2020). There are few studies on paleoclimates using element indicators in ancient deposits (e.g., Jurassic). Some trace element ratios in sediments are used to paleo-redox conditions, such as Ni/Co, U/Th, and V/(V + Ni) (Jones and Manning, 1994). The ratios of trace elements such as Rb/Sr can also be used to determine salinity (Lerman et al., 1995). The elements Sr and Cu ratio are often used to analyze the paleoclimate characteristics (Lerman et al., 1995). Ratios of Ni/Co, U/Th, Sr/Ba, and Sr/Cu are reliable indicators of paleoenvironment. The ratios of Ni/Co and U/Th are used to investigate the paleoenvironment, while the ratios of Sr/Ba and Sr/Cu indicate paleosalinity and paleoclimate, respectively.

5.2.1. *Paleosalinity*

Strontium and Ba have different geochemical behavior in sedimentary environments (Liu et al., 1984). Therefore, values and ratios of trace elements (e.g., B, Ba, and Sr) can be used to determine salinity (Lerman et al., 1995). The Sr/Ba ratio is one of the most widely used indicators

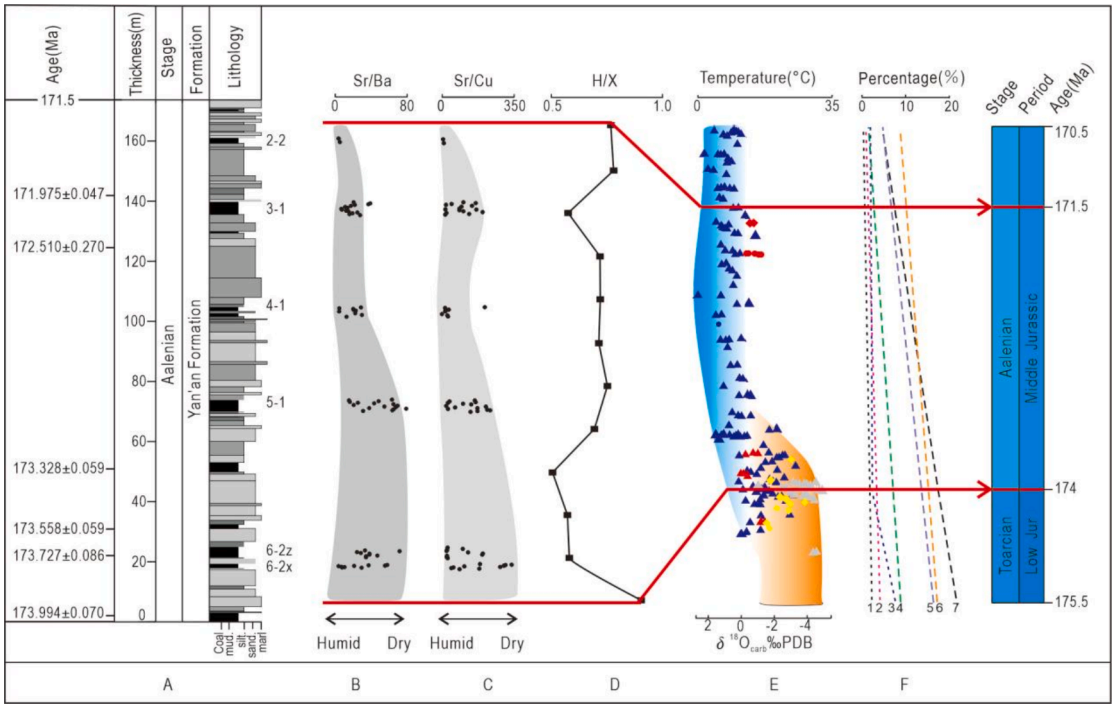

Fig. 7. Comparison of elementary proxies in the Yan'an Formation with other paleoenvironment records. (A) Stratigraphic column of the Yan'an Formation (Zhang et al., 2021). (B) Sr/Ba of the samples. (C) Sr/Cu of the samples. (D) Hygrophytic/Xerophytic (H/X) ratios of plant spores in Yan'an Formation (Sun et al., 2017). (E) Pliensbachian to Aalenian oxygen-isotope record plotted against subzone numbers. Shading behind the oxygen-isotope data highlights warm (red) and cool (blue) paleotemperature (Korte et al., 2015). (F) 1, 2, and 3 are contents of Cassopolis pollen from Western and Middle Siberia, southern regions of the former USSR, and the North fringe of the Asiatic part of the former USSR, respectively. 4, 5, 6, and 7 are, respectively, contents of thermophilous plants in China from North Xinjiang, Northwest China, Jingyuan, Gansu, and Qaidam basin (Deng et al., 2017b). (For interpretation of the references to colour in this figure legend, the reader is referred to the web version of this article.)

for sedimentary rocks and coals (Dai et al., 2020). High Sr/Ba value represents high salinity, while low Sr/Ba value represents low salinity (Deng and Qian, 1993).

The Sr/Ba ratio of the samples in the Yan'an Formation are all higher than 1, indicating the paleosalinity is generally high. The samples' relatively high Sr/Ba ratio at the bottom of the coal seam indicates a relatively high salinity during deposition of this portion of the coal. The Sr/Ba ratio decreases upward of the coal seam, reflecting decreasing salinity (Fig. 6A). The decrease in salinity from the bottom to the top of the seam may have been due to a decrease in the evaporation of water; the lesser concentration of water may indicate that the ancient temperature slowly decreased during the stage of Yan'an Formation deposition.

Generally, Sr/Ba values > 1 and < 1 indicate arid and humid climatic conditions, respectively (Dai et al., 2020). Therefore, the paleoclimate trends of the Yan'an Formation may indicate an intensification of humid conditions in this region.

5.2.2. *Depositional environment*

In addition to U, Mo, and V are also considered to be redox-sensitive, and several studies have utilized trace element ratios to evaluate paleo-redox conditions in sedimentary rocks (Dai et al., 2020). Generally, element ratios indicate environmental change (Mathews et al., 2020; Dai et al., 2020). Several authors have used the Ni/Co and U/Th ratios to indicate paleo-redox conditions (Rimmer, 2004).

Higher Ni/Co and U/Th ratios represent oxidizing conditions, whereas lower ratios suggest reducing conditions. Ni/Co > 7, Ni/Co $= 5 \sim 7$, Ni/Co < 5, respectively, indicate oxidizing, suboxic, and reducing environments (Dypvik, 1984). Jones et al. (1994) suggested that U/Th ratios of > 1.25, $0.75 \sim 1.25$, and < 0.75 indicate dysoxic, suboxic, and oxidizing conditions, respectively.

The Ni/Co ratios in the study samples of the Yan'an Formation are mostly lower than 7 (Fig. 6A), suggesting that the paleo-redox in this area is oxidic and suboxic. There are two Ni/Co mutation values at the top of 4–1 coal and 5–1 coal. There is no change of trend between the two anomalies and therefore discussed in this study. The U/Th ratio in the samples of the Yan'an Formation is all lower than 1.25 (Fig. 6A), indicating the paleo-redox in this area is oxidic. The interaction between Ni/Co and U/Th can infer that most samples were deposited in oxygen-rich or suboxidated redox environments (Fig. 6C).

5.2.3. *Paleoclimate*

The Sr/Cu ratio is susceptible to climate change (Xiong and Xiao, 2011). For example, Lerman et al. (1995) proposed that the Sr/Cu ratio of $1.3 \sim 5.0$ indicates warm and humid climate, and over 5.0 reflects drought conditions.

Rubidium has high stability during weathering, whereas Sr has low stability (Chen et al., 2000). During a warm climate with high precipitation, intense weathering can lead to a decreased trend in Sr content. Most of the Sr/Cu ratios of the Yan'an Formation coal samples are > 5. The vertical evolution of the Sr/Cu ratio indicates that the higher part of the seam was formed in a relatively warm and humid climate. The decrease of Sr/Cu ratio from lower Yan'an Formation to higher Yan'an Formation indicates even warmer and wetter weather conditions during deposition (Fig. 6A). The interaction between Sr/Cu and Sr/Ba can be used to infer that samples became warm and humid during deposition (Fig. 6B).

According to Zhang et al. (2016), the paleoclimate of the Yan'an Formation is interpreted to have been warm and humid from mudstone element indicators of the Yan'an Formation. Duan et al. (2013) and Jiang and Wang (2002) also determined that the sedimentary environment of the Yan'an Formation was warm and humid from the palynological assemblage. The trend of vertical climate change is evident in this study. This trend is consistent with the Sr/Ba indicators, which

further proves the accuracy of the result. The present study demonstrates that warmer and wetter conditions existed during the Yan'an Formation coal-bearing sequence deposition.

5.3. Relation between coal accumulation and early Aalenian global climate cooling event

The Jurassic world was long considered a warm and equable greenhouse climate, however, many rapid cooling events and even icehouse episodes have been identified (Dromart et al., 2003; Dera et al., 2011; Rogov and Zakharov, 2010), such as a drastic change in compiled $\delta^{18}O$ database (from well-dated bivalves and belemnites) for the Jurassic appears with calculated temperature variation exceeding 8 °C during the Toarcian-Aalenian transition (Dera et al., 2011). Recently, the Aalenian is considered to have been a Cool Mode during the Jurassic, with an abrupt mid-latitude cooling of seawater by as much as 10 °C; this is proposed to have been caused by the uplift of the North Sea Dome that impeded northward oceanic heat transport (Korte et al., 2015, and references therein) (Fig. 7E). However, the percentage changes of Classopollis pollen and thermophilous plants from Middle Jurassic deposits of the former USSR (Vakhrameev, 1991) and North China (Deng et al., 2017b) show that cooling and humid climate change occurred in the terrestrial area at that time (Fig. 7F). Consistent with this paleobotanical evidence, our Sr/Cu and Sr/Ba data of Yan'an Formation coal seams in the Ordos Basin also indicate climate change from a relatively arid condition to a more humid climate during the Aalenian (Fig. 7B-C), with more hygrophytic plants occurring in the upper Yan'an Formation (Sun et al., 2017) (Fig. 7D). Hence, the climate change in the mid-latitude terrestrial ecosystem could be the response to the significant change of marine environment during the Aalenian (Deng et al., 2017a). During cooling in an overall greenhouse state, the westerlies would be strengthened in mid-latitude Asia. As a result, global cooling during the Aalenian may have triggered strengthened moisture transport by westerlies in mid-latitude inland Asia, and therefore a humid climate in the Ordos Basin (Gao et al., 2015, 2021)

6. Conclusions

Based on the major and trace element analysis of the Middle Jurassic Yan'an coals of Ordos Basin, China, the following conclusions were drawn from our study:

1) The major element oxides in Yan'an coals are SiO_2 and CaO. In comparison with average values for China, the coals from the Ordos Basin have a slight enrichment of CaO and MgO. Sr and Mo are slightly higher than the average values for China. Yttrium and rare earth elements are depleted in the coals, and the distribution ranges between 7.92 μg/g to 268.56 μg/g with an average of 48.49 μg/g. A specific feature is the negative Eu anomaly in the Yan'an Formation coals which suggests that peat bog had stable terrigenous material supply during the coal-forming period.
2) It can be concluded that the paleoclimate was hot and dry with land-phase saltwater bodies and the oxygen-suboxygenic environment from the ratios of Sr/Ba, U/Th, Ni/Co, and Sr/Cu. However, the paleoclimate during the period of the Yan'an Formation was not a constant hot and arid climate. Instead, this study shows that the climate changed from arid to humid during the Aalenian of the Yan'an coal seam.
3) The Sr/Cu and Sr/Ba data of Yan'an Formation coal seams in the Ordos Basin indicate the climate change from a relatively arid condition to a more humid climate during Aalenian. Therefore, the climate change in the mid-latitude terrestrial ecosystem (e.g., Ordos Basin, North China) could be the response to the significant change of marine environment during the Aalenian. Global cooling during the Aalenian may have triggered strengthened moisture transport by westerlies in mid-latitude inland Asia, and therefore a humid climate in the Ordos Basin.

Declaration of Competing Interest

The authors declare that they have no known competing financial interests or personal relationships that could have appeared to influence the work reported in this paper.

Acknowledgements

This work was financially supported by the National Key R&D Plan of China (Grant No. 2017YFC0601405), the National Natural Science Foundation of China (Grant No. 41772096, 42102127), and the SDUST Research Fund (Grant No. 2018TDJH101).

References

Akhtar, S., Yang, X., Pirajno, F., 2017. Sandstone type uranium deposits in the Ordos Basin, Northwest China: A case study and an overview. Journal of Asian Earth Sciences 146, 367–382.
Ao, W., Huang, W., Weng, C., Xiao, X., Liu, D., Tang, X., Chen, P., Zhao, Z., Wan, H., Finkelman, R.B., 2012. Coal petrology and genesis of Jurassic coal in the Ordos Basin, China. Geoscience Frontiers 3, 85–95.
Bau, M., Dulski, P., 1996. Distribution of yttrium and rare-earth elements in the Penge and Kuruman iron-formations, Transvaal Supergroup, South Africa. Precambrian Research 79, 37–55.
Bhangare, R., Ajmal, P., Sahu, S., Pandit, G., Puranik, V., 2011. Distribution of trace elements in coal and combustion residues from five thermal power plants in India. International Journal of Coal Geology 86, 349–356.
Birk, D., White, J.C., 1991. Rare earth elements in bituminous coals and underclays of the Sydney Basin, Nova Scotia: Element sites, distribution, mineralogy. International Journal of Coal Geology 19, 219–251.
Boucot, A., Gray, J., 2001. A critique of Phanerozoic climatic models involving changes in the CO_2 content of the atmosphere. Earth-Science Reviews 56, 1–159.
Chang, S., Zhuo, J., Meng, S., Qin, S., Yao, Q., 2016. Clean coal technologies in China: current status and future perspectives. Engineering 2, 447–459.
Chen, J., Wang, Y., Chen, Y., Liu, L., Ji, J., Lu, H., 2000. Rb and Sr geochemical characterization of the Chinese Loess stratigraphy and its implications for palaeomonsoon climate. Acta Geologica Sinica-English Edition 74, 279–288.
Chermak, J.A., Schreiber, M.E., 2014. Mineralogy and trace element geochemistry of gas shales in the United States: Environmental implications. International Journal of Coal Geology 126, 32–44.
Dai, S., Bechtel, A., Eble, C.F., Flores, R.M., French, D., Graham, I.T., Hood, M.M., Hower, J.C., Korasidis, V.A., Moore, T.A., 2020. Recognition of peat depositional environments in coal: A review. International Journal of Coal Geology 219, 103383.
Dai, S., Graham, I.T., Ward, C.R., 2016. A review of anomalous rare earth elements and yttrium in coal. International Journal of Coal Geology 159, 82–95.
Dai, S., Ren, D., Chou, C.-L., Finkelman, R.B., Seredin, V.V., Zhou, Y., 2012. Geochemistry of trace elements in Chinese coals: a review of abundances, genetic types, impacts on human health, and industrial utilization. International Journal of Coal Geology 94, 3–21.
Dai, S., Finkelman, R.B., 2018. Coal as a promising source of critical elements: Progress and future prospects. International Journal of Coal Geology 186, 155–164.
Dai, S., Seredin, V.V., Ward, C.R., Hower, J.C., Xing, Y., Zhang, W., Song, W., Wang, P., 2015. Enrichment of U-Se–Mo–Re–V in coals preserved within marine carbonate successions: geochemical and mineralogical data from the Late Permian Guiding Coalfield, Guizhou, China. Mineralium Deposita 50, 159–186.
Dai, S., Xie, P., Jia, S., Ward, C.R., Hower, J.C., Yan, X., French, D., 2017. Enrichment of U-Re-V-Cr-Se and rare earth elements in the Late Permian coals of the Moxinpo Coalfield, Chongqing, China: Genetic implications from geochemical and mineralogical data. Ore Geology Reviews 80, 1–17.
Dai, S., Yan, X., Ward, C.R., Hower, J.C., Zhao, L., Wang, X., Zhao, L., Ren, D., Finkelman, R.B., 2018. Valuable elements in Chinese coals: A review. International Geology Review 60, 590–620.
Deng, S., Lu, Y., Zhao, Y., Fan, R., Wang, Y., Yang, X., Li, X., Sun, B., 2017a. The Jurassic palaeoclimate regionalization and evolution of China. Earth Science Frontiers 24, 106–142.
Deng, H., Qian, K., 1993. Sedimentary Geochemistry and Environmental Analysis. Science and Technology Press, Gansu (in Chinese with English abstract).
Deng, S., Zhao, Y., Lu, Y., Shang, P., Fan, R., Li, X., Dong, S., Liu, L., 2017b. Plant fossils from the Lower Jurassic coal-bearing formation of central Inner Mongolia of China and their implications for palaeoclimate. Palaeoworld 26, 279–316.
Dera, G., Brigaud, B., Monna, F., Laffont, R., Pucéat, E., Deconinck, J.-F., Pellenard, P., Joachimski, M.M., Durlet, C., 2011. Climatic ups and downs in a disturbed Jurassic world. Geology 39, 215–218.
Dromart, G., Garcia, J.-P., Picard, S., Atrops, F., Lécuyer, C., Sheppard, S., 2003. Ice age at the Middle-Late Jurassic transition? Earth Planetary Science Letters 213, 205–220.
Duan, J., Zhao, X., Ji, R., 2013. Sporopollen assemblage of the Middle Jurassic Yan 'an Formation in Dongsheng Coalfield, Inner Mongolia and its paleo-environmental significance. Science & Technology Information 126–127.

Dypvik, H., 1984. Geochemical compositions and depositional conditions of Upper Jurassic and Lower Cretaceous Yorkshire clays, England. Geological Magazine 121, 489–504.
Eskenazy, G.M., 1987. Rare earth elements in a sampled coal from the Pirin deposit, Bulgaria. International Journal of Coal Geology 7, 301–314.
Eterigho-Ikelegbe, O., Harrar, H., Bada, S., 2021. Rare earth elements from coal and coal discard–A review. Minerals Engineering 173, 107187.
Ferm, J., Horne, J., Weisenfluh, G., 1979. Carboniferous depositional environments in the Appalachian region. Carolina Coal Group, Columbia, South Carolina.
Jiang, D., Wang, Y., 2002. Middle Jurassic palynoflora and its environmental significance of Dongsheng, Inner Mongolia. Acta Sedimentologica Sinica 20, 47–54.
Johnson, E.A., Liu, S., Zhang, Y., 1989. Depositional environments and tectonic controls on the coal-bearing Lower to Middle Jurassic Yan'an Formation, southern Ordos Basin, China. Geology 17, 1123–1126.
Gan, H., Wang, H., Chen, J., Zhuang, X., Cao, H., Jiang, S., 2018. Geochemical characteristics of Jurassic coal and its paleoenvironmental implication in the eastern Junggar Basin, China. Journal of Geochemical Exploration 188, 73–86.
Gao, Yuan., Ibarra, D.E., Rugenstein, J.K.C., Chen, J., Kukla, T., Methner, K., Gao, Y., Huang, H., Lin, Z., Zhang, L., 2021. Terrestrial climate in mid-latitude East Asia from the latest Cretaceous to the earliest Paleogene: A multiproxy record from the Songliao Basin in northeastern China. Earth-Science Reviews 216, 103572.
Gao, Y., Ibarra, D.E., Wang, C., Caves, J.K., Chamberlain, C.P., Graham, S.A., Wu, H., 2015. Mid-latitude terrestrial climate of East Asia linked to global climate in the Late Cretaceous. Geology 43, 287–290.
Gayer, R., Rose, M., Dehmer, J., Shao, L.-Y., 1999. Impact of sulphur and trace element geochemistry on the utilization of a marine-influenced coal—case study from the South Wales Variscan foreland basin. International Journal of Coal Geology 40, 151–174.
Han, D., 1996. Coal petrology of China. China University of Mining and Technology press, Beijing (in Chinese with English abstract).
Hautevelle, Y., Michels, R., Malartre, F., Trouiller, A., 2006. Vascular plant biomarkers as proxies for palaeoflora and palaeoclimatic changes at the Dogger/Malm transition of the Paris Basin (France). Organic Geochemistry 37, 610–625.
Huang, G., Zhou, X., Wang, Z., 2009. Provenance Analysis of the Yan an Formation in Mid-Jurassic at the Southeast Area of Ordos Basin. Geochemistry Bulletin of Mineralogy, Petrology 28, 252–258.
Jones, B., Manning, D.A., 1994. Comparison of geochemical indices used for the interpretation of palaeoredox conditions in ancient mudstones. Chemical Geology 111, 111–129.
Ketris, M.P., Yudovich, Y.E., 2009. Estimations of Clarkes for Carbonaceous biolithes: World averages for trace element contents in black shales and coals. International Journal of Coal Geology 78, 135–148.
Kimura, T., 1998. Relationships between inorganic elements and minerals in coals from the Ashibetsu district, Ishikari coal field, Japan. Fuel Processing Technology 56, 1–19.
Korte, C., Hesselbo, S.P., Ullmann, C.V., Dietl, G., Ruhl, M., Schweigert, G., Thibault, N., 2015. Jurassic climate mode governed by ocean gateway. Nature Communications 6, 1–7.
Lerman, A., Imboden, D.M., Gat, J.R., Chou, L., 1995. Physics and chemistry of lakes. Springer-Verlag, Berlin.
Li, S., Yang, S., Kiewicz, T., 1995. Upper Triassic-Jurassic foreland sequence of the Ordos Basin in China in stratigraphic evolutions of foreland basin. SEPM Society for Sedimentary Geology 52, 214–233.
Liu, D., Zhou, A., Liu, J., 2007. Geochemical Characteristics of Rare Earth Elements in Yanan Formation, Jurassic System. Dongsheng Coalfield. Coal Geology of China 20–22, 43.
Liu, P., Huang, R., Tang, Y., 2019. Comprehensive understandings of rare earth element (REE) speciation in coal fly ashes and implication for REE extractability. Environmental Science Technology 53, 5369–5377.
Liu, Y., 1996. Simultaneous and precise determination of 40 trace elements in rock samples using ICP-MS. Geochimica 25, 552–558.
Liu, Y., Cao, L., Li, Z., 1984. Element geochemistry. Science and Technology Press, Bejing (in Chinese with English abstract).
Lv, D., Li, Z., Wang, D., Li, Y., Liu, H., Liu, Y., Wang, P., 2019. Sedimentary model of coal and shale in the paleogene Lijiaya formation of the Huangxian basin: insight from petrological and geochemical characteristics of coal and shale. Energy Fuels 33, 10442–10456.
Mathews, R.P., Pillai, S.S.K., Manoj, M., Agrawal, S., 2020. Palaeoenvironmental reconstruction and evidence of marine influence in Permian coal-bearing sequence from Lalmatia Coal mine (Rajmahal Basin), Jharkhand, India: A multi-proxy approach. International Journal of Coal Geology 224, 103485.
Qin, G., Liu, K., Xu, H., Ma, Z., Deng, L., Cao, D., 2015. Paragenetic Association Features of Trace Elements in Coals in Western Margin of Ordos Basin. Coal Geology of China 1–6, 18.
Rimmer, S.M., 2004. Geochemical paleoredox indicators in Devonian-Mississippian black shales, central Appalachian Basin (USA). Chemical Geology 206, 373–391.
Rogov, M., Zakharov, V., 2010. Jurassic and Lower Cretaceous glendonite occurrences and their implication for Arctic paleoclimate reconstructions and stratigraphy. Earth Science Frontiers 17, 345–347.
Scott, S., Anderson, B., Crosdale, P., Dingwall, J., Leblang, G., 2007. Coal petrology and coal seam gas contents of the Walloon Subgroup—Surat Basin, Queensland, Australia. International Journal of Coal Geology 70, 209–222.
Seredin, V.V., Dai, S., 2012. Coal deposits as potential alternative sources for lanthanides and yttrium. International Journal of Coal Geology 94, 67–93.
Sun, L., Zhang, Y., Zhang, T., Cheng, Y., Li, Y., Ma, H., Yang, C., Guo, J., Lu, C., Zhou, X., 2017. Jurassic sporopollen of Yan'an Formation and Zhiluo Formation in the northeastern Ordos Basin, Inner Mongolia, and its paleoclimatic significance. Earth Science Frontiers 24, 32–51.
Taylor, S., McLennan, S., 1985. The continental crust: its composition and evolution: an examination of the geochemical record preserved in sedimentary rocks using inductively coupled plasma source spectrometry. Chemical Geology 33, 141–153.
Vakhrameev, V.A., 1991. Jurassic and Cretaceous floras and climates of the Earth. Cambridge University Press, Cambridge.
Wang, Q., Yang, R., 2008. Study on REEs as tracers for late permian coal measures in Bijie City, Guizhou Province, China. Journal of Rare Earths 26, 121–126.
Wang, S., Lv, D., Tong, Y., Li, F., 1996. Coal accumulation law and coal resource evaluation in Ordos Basin. China Coal Industry Publishing House, Beijing (in Chinese with English abstract).
Wang, S., Zhang, Y., 1999. Study on the formation, evolution and coal-accumulating regularity of the Jurassic Ordos Basin. Earth Science Frontiers 6, 147–155.
Wang, X., Jiao, Y., Wu, L., Rong, H., Wang, X., Pan, S., Tang, H., Ji, B., Song, J., 2011. Major element geochemistry of Jurassic Coal in Dongsheng-Shenmu Area, Ordos Basin. Acta Sedimentologica Sinica 29, 520–528.
Wang, X., Wang, X., Pan, S., Yang, Q., Hou, S., Jiao, Y., Zhang, W., 2018. Occurrence of analcime in the middle Jurassic coal from the Dongsheng Coalfield, northeastern Ordos Basin, China. International Journal of Coal Geology 196, 126–138.
Wang, Y., Ren, D., Lei, J., Tang, Y., Yang, S., Yang, Y., 1997. Distribution of minor elements in Chinese coals. Scientia Geologica Sinica 32, 65–73.
Xiong, X., Xiao, J., 2011. Geochemical indicators of sedimentary environments-a summary. Earth Environment 39, 405–414.
Yin, L., Zhang, G., Zhang, G., 1990. Dongsheng Coalfield geological data compilation (No. 6802) [in Chinese]. The National Geological Archives of the China Geological Survey. http://www.ngac.cn.
Zhang, H., Baidu, Q., Zhang, X., Gao, Z., He, X., Li, H., Lu, Z., 1995. Formation of the Ordos Basin and Its coal-forming Tectonic Environment. Coal Geology Exploration 3, 1–9.
Zhang, T., Sun, L., Zhang, Y., Cheng, Y., Li, Y., Ma, H., Lu, C., Yang, C., Guo, G., 2016. Geochemical characteristics of the Jurassic Yan'an and Zhiluo Formations in the northern margin of Ordos Basin and their paleoenvironmental implications. Acta Geologica Sinica 90, 3454–3472.
Zhang, Z., Wang, T., Ramezani, J., Lv, D., Wang, C., 2021. Climate forcing of terrestrial carbon sink during the Middle Jurassic greenhouse climate: Chronostratigraphic analysis of the Yan'an Formation, Ordos Basin, North China. Geological Society of America Bulletin 133, 1723–1733.
Zhao, C., Duan, D., Li, Y., Zhang, J., 2012. Rare earth elements in No. 2 coal of Huangling mine, Huanglong coalfield. China. Energy Exploration Exploitation 30, 803–818.